Extricating dynamic topography from subsidence patterns: Examples from Eastern North America's passive margin

Matthew Morris[a], Victoria Fernandes[a], Gareth G. Roberts[a]

[a]*Department of Earth Science and Engineering, Imperial College London, South Kensington Campus, SW7 2AZ, UK, gareth.roberts@imperial.ac.uk.*

Abstract

Global sea-level (eustatic) histories generated by backstripping stratigraphy are predicated upon the lithosphere having a well understood tectonic history. However, sub-plate processes play a role in governing lithospheric vertical motions with timescales and amplitudes akin to eustasy, which are difficult to predict. We examine how stratigraphic and geophysical observations combined with simple isostatic models can be used to disentangle histories of sub-plate support and eustasy. We focus on the passive margin of Eastern North America, where a generally accepted history of eustasy has been estimated. Negative long wavelength free-air gravity anomalies, residual ocean-age depth estimates, fast upper mantle shear wave velocities, and geodynamic models suggest that Cenozoic evolution of this passive margin has been influenced by upper mantle drawdown. We build on existing analyses to backstrip sixteen wells, which, combined with seismic data, constrain timing and extent of Cenozoic subsidence. Results indicate up to $\sim$ 600 m of water-loaded subsidence between $\sim$ 20–0 Ma centered on the Baltimore Canyon Trough. Seismic data from the trough shows Neogene aggrading clinoforms. There is little evidence for faulting or stratigraphic growth, which indicates that Neogene lithospheric strain rates were low. Amplitude and spatial extent of Neogene subsidence are difficult to explain by glacio-eustasy or glacio-isostatic adjustment. Instead, sub-plate support calculated from conversion of shear wave velocities to temperature and isostatic calculations indicate that upper mantle drawdown was responsible for subsidence of the margin. Because mantle convection is vigorous such observations are expected throughout the stratigraphic archive.

Keywords: Mantle convection, subsidence, sea level, eustasy, Neogene, New Jersey margin

1. Introduction

It is generally accepted that mantle convection can generate time-dependent vertical motions of the lithosphere that overlap in amplitude and timescale with estimates of eustatic (global) sea-level change ($O(10^1–10^2)$ m, $O(10^{-1}–10^2)$ Ma; Hager et al., 1989; Lithgow-Bertelloni and Silver, 1998; Miller et al., 2005; Hartley et al., 2011; Rovere et al., 2014; Cloetingh and Haq, 2015; Kominz et al., 2016). Stratigraphy and sub-plate shear wave velocities from the Mauritanian margin of northern Africa and Australian's Northwest Shelf, for example, indicate that mantle convective drawdown can generate hundreds of meters of water-loaded subsidence on timescales of 1–10 Ma (Czarnota et al., 2014; Lodhia et al., 2018). Residual ocean age-depth measurements indicate that dynamic topography has wavelengths of hundreds to thousands of kilometers and amplitudes of up to $O(10^3)$ m (Hoggard et al., 2017). These observations and the complex response of sea level to glacial unloading means that estimating eustasy from a single site is generally challenging (see e.g. Austermann et al., 2017). Given the general importance of accurately constraining sea-level change we examine how geological data can be used to disentangle histories of dynamic support from eustasy. We investigate whether a signal of sub-plate support can be isolated using stratigraphic and geophysical observations along Eastern North America's passive margin, where eustasy has been studied (Figure 1; e.g. Miller et al., 2005; Kominz et al., 2016). First, geophysical observations (e.g. gravity, tomography, ocean age-depth measurements) are used to assess present-day flexural, lithospheric and sub-plate support of topography along the eastern margin of North America. Secondly, the stratigraphic archive is used to examine the history of lithospheric vertical motion.

The stratigraphic record at passive margins can be affected by a suite of geological processes including the history of rifting and post-rift cooling, eustasy, sub-plate support and the effects of water-loading and glacial unloading (e.g. McKenzie, 1978; Le Pichon and Sibuet, 1981; Lambeck and Chappell, 1988; Allen and Allen, 2005; Kominz et al., 2016; Austermann

et al., 2017; Müller et al., 2018). One approach to circumvent the challenging task of isolating, for example eustasy, is to backstrip stratigraphy at margins with a well understood tectonic (e.g. rift and post-rift) history (e.g. Miller et al., 2003; Kominz et al., 1998, 2016). The eastern seaboard of North America has been used to do so because its tectonic history is, on the whole, well understood (e.g. Watts and Ryan, 1976; Steckler and Watts, 1978; Watts and Thorne, 1984). Biostratigraphic analyses of core and cuttings from wells along the margin combined with reflection and refraction seismology, and oceanic magnetic anomalies, show that, following late-Triassic to early-Jurassic rifting, post-rift subsidence of the margin has been governed principally by lithospheric cooling (e.g. Steckler and Watts, 1978; Grow et al., 1988; Miller et al., 2005, 2013; Kominz et al., 2008, 2016; Greene et al., 2017). Fitting of simple cooling models to backstripped subsidence patterns and inversion for strain rate histories indicate that the lithosphere beneath the extensively studied COST B-2 well in the Baltimore Canyon Trough stretched by a factor, $\beta \sim 2$ (e.g. Flament et al., 2013). However, stratigraphy of the deepest (syn-rift) parts of this margin is sparsely sampled and this value is debated (see e.g. Watts and Thorne, 1984). Residual subsidence has been interpreted as changes in accommodation space caused by eustasy (e.g. Miller et al., 2005). Additional mechanisms proposed to generate subsidence along this margin include a flexural response due to loading, plate reorganisation and epeirogeny generated by dynamic support (Cloetingh et al., 1990; Pazzaglia and Gardner, 1994; Vanderaveroet, 2000; Browning et al., 2006; Kominz et al., 2008, 2016). A suite of geodynamic models predict mantle convective drawdown of the margin with amplitudes up to $O(10^3)$ m and wavelengths up to $O(10^4)$ km (e.g. Spasojević et al., 2008; Müller et al., 2008; Moucha et al., 2008; Flament et al., 2013; Steinberger et al., 2017). Some of these models predict tens to hundreds of meters of Neogene dynamic support of the New Jersey margin (e.g. Moucha et al., 2008; Spasojević et al., 2008; Flament et al., 2013). However, there is disagreement on the predicted timing, amplitude and wavelength of support and whether sub-plate processes have generated uplift or subsidence.

In this study we combine backstripping of sixteen wells along Eastern North America's passive margin with seismological and gravity data and simple isostatic calculations to estimate the timing, amplitude and wavelength of sub-plate support. We start by summarising geophysical observations that constrain present-day dynamic support.

2. Gravity, ocean age-depth residuals and tomography

Figure 1b shows free air gravity data extracted from the GRACE dataset filtered to remove wavelengths $\lesssim$ 800 km, which is a guide to sub-plate support (e.g. McKenzie, 2010; Colli et al., 2016). The Baltimore Canyon Trough has negative free-air gravity anomalies of between ~ -30 to 0 mGal (Tapley et al., 2005). In comparison, the Georges Bank and the Southeast Georgia Embayment, $\sim$ 500 km north and $\sim$ 1000 km south of the trough, respectively, have anomalies of $\sim$ 0 to +10 mGal. Positive free-air anomalies are centered on the Bermuda Rise and on the Appalachian mountains (e.g. Courtillot et al., 2003). If a transfer function of 30–50 mGal km^{-1}, which encompasses the range of admittance values typically assumed for oceanic and continental dynamic support, is used to convert long wavelength gravity into a prediction of sub-plate support it implies that the Baltimore Canyon Trough is drawn down by $\sim$ 0.6–1 km today (Crosby et al., 2006). Calculated drawdown does not extend to the Georges Bank or the Southeast Georgia Embayment (Figure 1b). These results are broadly consistent with some geodynamic predictions of upper mantle convective drawdown (e.g. Steinberger et al., 2017). Nevertheless, we acknowledge that using single admittance values to estimate dynamic support is debated (see e.g. Colli et al., 2016). Admittance methods indicate that the elastic thickness of Eastern North America's continental lithosphere is $O(10)$ km (e.g. McKenzie, 2010). Recent spherical wavelet transformation of gravity and topography indicate that the elastic thickness of Eastern North America's passive margin is $\sim$ 15–40 km, which implies that sub-plate processes could be manifested at Earth's surface at wavelengths $O(100)$ km (Audet and Bürgmann, 2011; Audet, 2014).

Residual ocean age-depth measurements can also be used to estimate sub-plate support (Figure 1c; Hoggard et al., 2017). Oceanic lithosphere close to the Baltimore Canyon Trough has a residual depth of -0.2 to -0.4 km. Highest positive residuals in this region (almost $+1$ km) are centered on the Bermuda Rise.

A slice through the SL2013sv shear wave tomography model at 125 km depth beneath eastern North America and the western Atlantic Ocean is shown in Figure 1d (Schaeffer and Lebedev, 2013). Upper mantle velocity anomalies appear to be a few percent faster than the AK135 global model beneath the Baltimore Canyon Trough. A suite of other recent shear wave tomographic models also shows fast upper mantle velocity anomalies beneath the New Jersey margin (Supplementary Material; Ritsema et al., 2011; Moulik and Ekstrom, 2014; French and Romanowicz, 2014; Durand et al., 2017). The SL2013sv model has broadly comparable velocities to the global average beneath the Southeast Georgia Embayment and the Georges Bank. A long wavelength slow velocity anomaly is centered on the Bermuda Rise. We note that sub-plate support calculated from gravity and residual ocean-age depths also broadly correlate with upper mantle velocity anomalies in more recent shear wave tomographic models improved by data collected during the EarthScope Transportable Array experiment (Figure 1; Clouzet et al., 2018). These observations combine to suggest that the Baltimore Canyon Trough sits on the margins of upper mantle that is drawing down the lithosphere. Whereas sub-plate uplift or drawdown of the Georges Bank and Southeast Georgia Embayment appears to be negligible (Figure 1).

Many, but not all, geodynamic models of mantle convection predict dynamic drawdown of most of the margin during the last ~ 30 Ma (e.g. Forte et al., 2007; Moucha et al., 2008; Spasojević et al., 2008; Spasojević and Gurnis, 2012; Müller et al., 2018). These models tend to emphasise the importance of flow at deeper, mid-mantle, depths associated with Farallon plate subduction in driving drawdown. Gravity and residual ocean age-depth data, and more recent tomographic models indicate that support of the margin might be related to upper

mantle structure (e.g. Figure 1). In other places (e.g. West Africa, Northwest Australia, Borneo) dynamic topography appears to be governed by the thermal (buoyancy) structure of the uppermost convecting mantle (e.g. Czarnota et al., 2014; Hoggard et al., 2017; McNab et al., 2018; Roberts et al., 2018; Lodhia et al., 2018).

In order to estimate the history of drawdown of Eastern North America's passive margin, first, we calculate the subsidence histories of sixteen wells from Georges Bank to the Southeast Georgia Embayment. Secondly, we calculate the contribution of excess upper mantle temperature anomalies to surface elevations by converting shear wave velocities to temperature and performing simple isostatic calculations. Finally, we examine the importance of these results for eustasy.

3. Wells, backstripping and seismic data

Sixteen wells along the Atlantic continental margin, including the COST B-2 well, were backstripped to calculate their subsidence histories (Figure 2). Thirteen of these wells are located in, or are proximal to, the Baltimore Canyon Trough. The COST G-1 and COST G-2 wells are located on Georges Bank, and the COST GE-1 well is in the Southeast Georgia Embayment.

Stratigraphy was backstripped using a one-dimensional model that assumes Airy isostasy, which is probably appropriate because this stretched margin has an elastic thickness, $T_e \sim$ 15–40 km (e.g. Watts and Ryan, 1976; Audet, 2014). Age-depth relationships were determined by biostratigraphic correlation of foraminifera, nannofossils and palynomorphs recorded in published well logs (see summary in Figure 3). Palaeowater depths, interpreted from benthic fauna, were extracted from the well reports (Figure 3; Supplementary Information).

Once age-depth relationships were obtained the wells were backstripped, decompacted and water-loaded to isolate the signal of tectonic subsidence. Where available, checkshot data was used to determine initial porosity, $\phi_\circ$, and compaction wavelength, λ. Calculated porosity-depth curves were compared to available porosity measurements (e.g. Figure 4c–d; Supplementary Material). First, we sought the $\phi_\circ$ and λ values that yielded calculated time-depth pairs with the lowest residual misfit to checkshot values. Porosity as a function of depth was parameterized using Athy (1930)'s well-known formulation

$$\phi(z) = \phi_\circ \exp\left(-\frac{z}{\lambda}\right). \tag{1}$$

Velocity, v_s, as a function of porosity (and depth), which can be straightforwardly related to time-depth pairs, was calculated using Wyllie et al. (1956)'s approach

$$\frac{1}{v_s(z)} = \frac{\phi(z)}{v_w} + \frac{1-\phi(z)}{v_{sg}}. \tag{2}$$

Here, v_w represents pore fluid velocity and was assigned a value of 1.5 km s^{-1}, representative of seawater, and v_{sg} is the solid grain velocity, assigned a value of 5.5 km s^{-1} to represent a sand-clay mixture, which is appropriate for wells in the Baltimore Canyon Trough (see e.g. Kominz et al., 2016). Two-way travel time, T, and velocity are related such that

$$\int_0^T \mathrm{d}t = 2\int_0^z \frac{\mathrm{d}z}{v_s(z)}, \tag{3}$$

and by combining Equations 1 and 2 and substituting into Equation 3, yields

$$T = 2\left\{\lambda\phi_\circ\left[\frac{1}{v_{sg}} - \frac{1}{v_w}\right]\left[\exp\left(\frac{-z}{\lambda}\right) - 1\right] + \frac{z}{v_{sg}}\right\}. \tag{4}$$

$\phi_\circ$ and λ were systematically varied to determine the minimum misfit between observed checkshot data and calculated time-depth curves (Figure 4; Supplementary Material). Where checkshot data was not available, an initial porosity of 0.6 and compaction wavelength of 2 km were assumed (Steckler and Watts, 1978; Kominz et al., 2016).

Assuming that the total amount of solid material remains constant during compaction, the decompacted thickness of each sedimentary layer is

$$\int_{z_1}^{z_2} [1-\phi(z)]\mathrm{d}z = \int_{z_3=0}^{z_4} [1-\phi(z)]\mathrm{d}z, \tag{5}$$

where $z_2 - z_1$ and $z_4 - z_3$ are sedimentary layer thicknesses before and after compaction, respectively. Substitution with Equation 1 and solving the integral gives

$$z_4 = z_2 - z_1 + \phi_\circ \lambda \left[\exp\left(-\frac{z_2}{\lambda}\right) + \exp\left(-\frac{z_1}{\lambda}\right) + 1 - \exp\left(-\frac{z_4}{\lambda}\right) \right]. \quad (6)$$

z_4 is solved iteratively for each layer using the Newton-Raphson method. The resultant decompacted subsidence curves are then standardised assuming Airy isostasy and a water load, such that

$$S_w = S_s \left(\frac{\rho_a - \rho_s}{\rho_a - \rho_w} \right). \quad (7)$$

Where S_w and S_s are water and sediment loaded subsidence, respectively. If asthenospheric density, $\rho_a = 3200$ kg m^{-3}, average sediment density, $\rho_s = 2400$ kg m^{-3}, and water density, $\rho_w = 1000$ kg m^{-3}, Equation 7 simplifies to $3S_w \approx S_s$. Figure 4d shows calculated $\phi_\circ$ and λ values for the COST B-2 well compared to porosity-depth data acquired from core and cuttings (Steckler and Watts, 1978; Watts and Thorne, 1984; Van Sickel et al., 2004). The porosity-depth relationship calculated from check-shot data broadly matches these independent observations and suggests that a simple calibrated parameterization of compaction is justified. We note that shallow wells tend to emphasize subsidence anomalies since no underlying stratigraphy is included in the decompaction procedure. An additional source of uncertainty in subsidence histories is palaeowater depth. Figure 3 shows a summary of palaeowater depths in the Baltimore Canyon Trough synthesised from well reports. Our results indicate that Late Jurassic to Recent water depths have varied between upper bathyal to neritic, which is consistent with other interpretations (e.g. Kominz et al., 2016).

3.1. Theoretical thermal subsidence

The predictability of passive margin subsidence and its relationship to strain and lithospheric cooling is well known (e.g. McKenzie, 1978; White, 1994). It forms the basis for extracting eustasy from backstripped stratigraphy (e.g. Watts and Ryan, 1976; Miller et al., 2005; Kominz et al., 2016).

A challenging problem along this margin is that its deep structure, and therefore the timing of rifting, are poorly understood, partly because nearly all wells terminate in post-rift stratigraphy (see e.g. Grow et al., 1983; Watts and Thorne, 1984; Sheridan et al., 1993). A guide to the time at which continental stretching (rifting) terminated is the age of oldest abutting oceanic crust. Greene et al. (2017) suggest that if the source of the Blake Spur Magnetic Anomaly is oceanic crust it may have formed at $\sim$ 168.5 Ma, which gives a basis for assuming rifting terminated before then. However, there is some debate about the age and origin of the oldest magnetic isochron offshore eastern North America (see Greene et al., 2017). Seismic and geophysical data indicate that 0.5–3.7 km of sedimentary rock sits atop the rifted basement of the Baltimore Canyon Trough (e.g. Benson and Doyle, 1988). Diagnostic Late Triassic dinoflagellates from the deepest sampled stratigraphy in the COST G-2 well on Georges Bank correlate with the oldest sedimentary rock preserved in half-graben onshore (e.g. Newark Supergroup), which suggests that the earliest sediment to fill on- and offshore basins did so contemporaneously (Cousminer, 1983).

Onshore, the Newark supergroup comprises continental clastic and extrusive volcanic rocks preserved within asymmetric half-grabens that crop out along the coastal plain (e.g. Newark-Gettysburg, Culpeper, Richmond, Hartford and New York Bight basins; Manspeizer, 1988). Biostratigraphic analysis of fossil plants, pollens and spores from these sedimentary rocks indicate that these graben are Upper Triassic aged ($\sim$ 227 Ma; Cornet and Olsen, 1985). Radiometrically-dated tholeiitic lavas that are interbedded within lacustrine grow strata provide additional constraints on the timing of rifting (e.g. Orange Mountain, Aspers, Watchung and Deerfield basalts). They have U-Pb and $^{40}Ar/^{39}Ar$ ages of 201 ± 1 Ma, and K-feldspar cements formed from hydrothermal fluids generated during magamtism have $^{40}Ar/^{39}Ar$ ages of 196 ± 1 Ma (Weems and Olsen, 1997). A complicating factor is that some of these igneous rocks were later hydrothermally altered, which can make the calculated ages of these rocks appear younger than their true ages (Seidemann et al., 1984; Sutter, 1988). Offshore, syn-rift sedimentary rock is separated from thick post-rift stratigraphy by a regional angular unconformity, which is observed on two-dimensional seismic profiles as a

strong reflector with onlapping younger sedimentary packages (see e.g. Grow et al., 1983). Palynomorphs from the COST G-2 well indicate that this regional unconformity was generated during Lower Jurassic times (Cousminer and Steinkraus, 1988). These observations give a basis for assuming that rifting occurred between $\sim$ 230–170 Ma (Upper Triassic to Lower Jurassic).

Stratigraphy from the COST B-2 well has been combined with inferences about the deep structure of the margin to invert syn-rift to Recent subsidence patterns for strain rate histories, $\dot{\epsilon}(t)$, which indicate lithospheric stretching factor $\beta = \exp(\int_{\circ}^{t} \dot{\epsilon}(t)\mathrm{d}t) \sim 1.7$–$2.2$ (see e.g. Watts and Thorne, 1984; Jarvis and McKenzie, 1980; Grow et al., 1988; White, 1994; Kominz et al., 1998; Flament et al., 2013).

An alternative pragmatic approach to dealing with a poorly constrained syn-rift history is to constrain stretching factors and rifting histories by comparing root-mean-squared misfit between observed and theoretical thermal subsidence histories generated by systematically varying stretching factors and the timing of rifting. We make use of simple analytical solutions that assume instantaneous stretching and relate β, asthenospheric temperature (T), thermal expansivity (α), lithospheric density (ρ_m), and infill (e.g. water; ρ_w), time since rifting (t), and the thermal time constant of the lithosphere ($\tau = l^2/(\pi^2\kappa)$) to calculate thermal subsidence (S_t) histories

$$S_t = E_{\circ} r \left[1 - \exp\left(-\frac{t}{\tau}\right)\right], \quad \text{where} \tag{8}$$

$$E_{\circ} = \frac{4 l \rho_m \alpha T}{\pi^2(\rho_m - \rho_w)} \quad \text{and} \quad r = \frac{\beta}{\pi} \sin\left(\frac{\pi}{\beta}\right). \tag{9}$$

We set lithospheric thickness, $l = 125$ km, thermal diffusivity, $\kappa = 10^{-6}$ m^2 s^{-1}, $\rho_m = 3300$ kg m^{-3}, $\alpha = 3.28 \times 10^{-5}$ /°K, and $T = 1330$°C. We systematically varied $1 \leq \beta \leq 5$ and timing of rifting, $t_{\circ}$, between 250–170 Ma to calculate the best-fitting values for the COST B-2 well (Supplementary Material). Stretching factors and the timing of rifting tradeoff such that $2 \leq \beta \leq 5$ and $170 \leq t_{\circ} \leq 200$ Ma yield low misfits. These values overlap results from inverting subsidence patterns, probably because the duration of rifting was short (i.e. $\sim$ 15–25 Ma; Jarvis and McKenzie, 1980; Flament et al., 2013).

Substituting $1.7 \leq \beta \leq 2.2$ and $170 \leq t_\circ \leq 200$ Ma into Equations 8 and 9 yields total water-loaded thermal subsidence since rifting of 1876 ± 281 m, which brackets post-rift subsidence recorded by backstripping of the COST B-2 well (blue curve in Figure 4). Calculated Neogene to Recent (23–0 Ma) thermal subsidence is 31 ± 13 m. The proximity of the margin to the Appalachian mountains and thick lithosphere imaged in some shear wave tomographic models indicates that the lithosphere beneath this margin might have been thicker before stretching. If, for example, $l = 150$ km calculated Neogene water loaded subsidence is 71 ± 24 m. These values of calculated Neogene thermal subsidence are nearly an order of magnitude lower than observed values ($\sim$ 500–600 m; e.g. Figures 4 & 5).

Neogene stratigraphy was mapped along the margin using six two-dimensional seismic reflection lines (Figures 2 & 6; Supplementary Information). These lines were chosen because of their proximity to backstripped wells, image fidelity and so that stratigraphy could be interpreted on dip and strike lines. Seismic stratigraphy was tied to wells with accurate, biostratigraphically determined, ages. Age constraints from each well were converted from depth into two-way travel times using checkshot data and interval velocities provided in the well reports (Figure 3).

4. Results

Figure 4 shows the subsidence profile for the COST B-2 well. This figure also shows the eustatic curve of Miller et al. (2005), which was generated by identifying residuals (i.e. non-tectonic subsidence) from backstripped stratigraphy, and correlation with oxygen isotopic time series (Van Sickel et al., 2004). The analyses in this paper differ from Miller et al. (2005) in that we do not assume residual subsidence is necessarily generated by eustasy. Cumulative water-loaded subsidence from 188 Ma to the present day is 2.4 km. Most of this subsidence can be attributed to post-rift thermal sag (e.g. Equations 8 & 9). The most significant departure from predicted post-rift subsidence is between 20–11 Ma when an additional $\sim$ 200–500 m of water-loaded subsidence is observed. Flament et al. (2013)

also observed an increase in Neogene subsidence rates, which they show could be attributed to increased lithospheric strain (i.e. stretching) centered at $\sim$ 16 Ma or mantle convective drawdown (e.g. their Figures 6 & 7). Figure 5 shows subsidence profiles for all wells in this study. Anomalous water-loaded Neogene subsidence, with rates of up to $\sim$ 50 m Ma^{-1} between $\sim$ 20–0 Ma, is observed for most wells in the the Baltimore Canyon Trough and for the Bethany Beach well onshore. The sparsely populated subsidence curves shown in Figures 5i-k are a result of scant post-Cretaceous stratigraphic information. These wells have high residual post-Cretaceous subsidence, which is broadly comparable to that recorded in the more completely sampled wells. However, the sparsity of reported Cenozoic stratigraphy means that Neogene subsidence rates are not well constrained and they are excluded from subsequent analyses. The age of stratigraphy sampled during IODP Expedition 313 ages is determined by Sr isotopic chemistry and has a resolution of $\pm$0.25–0.5 Ma (Kominz et al., 2016). Backstripping of these wells shows that subsidence rates increased between 20 and 13 Ma (Figures 5e-g; Kominz et al., 2016). In contrast, wells located on Georges Bank and the Southeast Georgia Embayment have $\lesssim$ 1 km of post-Santonian stratigraphy and almost no residual Neogene water-loaded subsidence (Figure 5a, b, o).

Seismic data and biostratigraphic correlations indicate that Neogene to Recent stratigraphy is up to $\sim$ 1 s thick (two-way time; $\sim$ 1 km) in the Baltimore Canyon Trough (Figures 4c & 6). Strike line A-148, which intersects the trough, shows that Miocene to Recent stratigraphy is almost uniformly planar and $>$ 1 s thick offshore New Jersey (Supplementary Information). In contrast seismic lines MMG16 and LMG81 on Georges Bank show that post-Santonian ($\lesssim$ 84 Ma) stratigraphy is $<$ 1 s thick. Well COST GE-1 on the bank indicates that its Miocene to Recent stratigraphy is $<$ 100 m thick. Post-Jurassic stratigraphy of Georges Bank has a shallow gradient in strike and dip directions (Supplementary Information). In contrast, dip lines from the Baltimore Canyon Trough show $>$ 100 km of Miocene-Recent progradation and $\sim$ 0.25 s ($\sim$ 250 m) of aggradation (Figure 6; Supplementary Information). These clinoforms prograde from close to the shoreline and are best developed in the northern

part of the Baltimore Canyon Trough. Rapid increases in accommodation space offshore was coeval with increased sedimentary flux from onshore (e.g. Poag and Sevon, 1989).

5. Discussion

Up to $\sim$ 600 m of Neogene to Recent ($\sim$ 20–0 Ma) water-loaded subsidence is recorded by backstripped wells centered on the Baltimore Canyon Trough. Seismic strike line A-148, which intersects the trough, shows that accumulation of Neogene sedimentary rock is up to $\sim$ 1 s ($\sim$ 1 km) along at least $\sim$ 200 km of the margin offshore New Jersey (Supplementary Information). Miocene clinoforms, mapped on seismic dip lines, prograded $>$ 100 km away from the coastline and then aggraded, which indicates an increase in Neogene accommodation space (see e.g., seismic lines DS11, LMB10; Greenlee et al., 1988; Posamentier et al., 1988; Poag and Sevon, 1989; Greenlee et al., 1992). Neogene clastic sedimentary rock was probably generated as a consequence of Miocene uplift and enhanced erosion of the Appalachian mountains (cf. Poag and Sevon, 1989; Monteverde et al., 2008; Roberts et al., 2012). In contrast, seismic mapping and backstripped stratigraphy on the Georges Bank and the Southeast Georgia Embayment shows that Neogene subsidence and sedimentation rates were much lower. These observations imply that the relatively rapid Neogene to Recent subsidence observed in the Baltimore Canyon Trough is a local, rather than global (e.g. eustatic), phenomenon. The amplitude of water-loaded Neogene subsidence in the Baltimore Canyon Trough (up to $\sim$ 600 m) also precludes glacio-eustasy as the mechanism for increased accommodation space along this margin. In the following section, we examine whether observed subsidence patterns could have been generated by flexure, lithospheric strain or sub-plate support.

5.1. A role for plate flexure or extension?

Subsidence of the Baltimore Canyon Trough has been previously attributed to a flexural response to loading (Pazzaglia and Gardner, 1994; Kominz et al., 1998; Vanderaveroet, 2000;

Kominz et al., 2008; Miller et al., 2013). We use a simple flexural model to examine whether loading could have generated the observed water-loaded subsidence patterns in the trough and its surroundings. Our flexural model assumes that the lithosphere deflects as a semi-infinite plate in response to an end load. Maximum deflection, $w_\circ = V_\circ \alpha^3/4D$, where the flexural parameter, α, and flexural rigidity, D, are given by

$$\alpha = \left[\frac{4D}{g(\rho_m - \rho_w)}\right]^{\frac{1}{4}}, \qquad D = \frac{ET_e^3}{12(1-\sigma^2)}, \tag{10}$$

(e.g. Turcotte and Schubert, 2002). Gravitational acceleration, $g = 9.8$ m s^{-2}, mantle density, $\rho_m = 3300$ kg m^{-3}, water density, $\rho_w = 1000$ kg m^{-3}, Youngs Modulus, E = 70 GPa, and Poisson's ratio $\sigma = 0.25$. The most obvious nearby large load is the Appalachian mountains. We estimate the width of foreland basins for a range of elastic thicknesses by calculating the position of forebulges, x_b, relative to the eastern edge of the Appalachian mountains using $x_b = 3\pi\alpha/4$ (Turcotte and Schubert, 2002). Figure 8 shows the distance to the forebulge from the eastern edge of the mountains for elastic thicknesses of 20–40 km (cf. Watts and Ryan, 1976; Pazzaglia and Gardner, 1994; McKenzie, 2010; Audet, 2014). These tests indicate that loading by the Appalachian mountains did not generate the observed Neogene subsidence. To produce a forebulge to the east of the Baltimore Canyon Trough requires an elastic thickness of $\gtrsim$ 100 km, which is much higher than that estimated from the admittance between gravity and topography along the margin ($\sim$ 15–40 km; Watts and Ryan, 1976; McKenzie, 2010; Audet and Bürgmann, 2011; Audet, 2014).

Another way to generate relatively rapid Neogene subsidence could be increasing lithospheric strain rates (stretching). Inversion of the subsidence history of the COST B-2 well indicates that Neogene strain rates of up to $\sim$ 5 Ga^{-1} are required to generate observed subsidence patterns (Flament et al., 2013). However, seismic lines in the Baltimore Canyon Trough do not show obvious faulting, or Neogene stratigraphic growth, which precludes lithospheric extension as an important mechanism for generating subsidence at this time. An obvious next step is to investigate the role sub-lithospheric support might play in generating lithospheric subsidence.

5.2. Sub-plate support

Several geodynamic models predict post-Cretaceous dynamic topography along the east coast of North America (e.g. Moucha et al., 2008; Spasojević et al., 2008; Flament et al., 2013; Liu, 2015). Most of these models use broadly similar techniques to convert seismic tomographic models into predictions of mantle flow. Many predict dynamic support of the margin at wavelengths in excess of 1000 km. Moucha et al. (2008) calculated dynamic uplift of 100–200 m over the past 30 Ma. In contrast, Spasojević et al. (2008) estimated 100–200 m of dynamic drawdown over the same period and Müller et al. (2008) propose subsidence of 105–385 m since 70 Ma. Flament et al. (2013)'s model predicts 580 m of subsidence since 80 Ma, and $\sim$ 30 m since 15 Ma, whilst Rowley et al. (2013) estimate uplift of +10–20 m since 3 Ma. Dynamic uplift or subsidence along this margin is usually attributed to subduction of the cold, dense, relict Farallon slab, which is generally thought to reside in the lower mantle ($\gtrsim$ 670 km depth; see e.g. Rowley et al., 2013; Liu, 2015).

Instead, we suggest that long wavelength free-air gravity anomalies, residuals ocean age-depth measurements, upper mantle shear wave tomography, and the stratigraphic and subsidence history of the margin suggest that Neogene dynamic drawdown was centered on the Baltimore Canyon Trough and extended not more than $\sim$ 500 km away from it (e.g. Figures 1 & 7). These observations indicate that the shallow upper mantle might be playing an important role in generating dynamic support of the the margin (e.g. Figure 1; Colli et al., 2016; Hoggard et al., 2017; Lodhia et al., 2018; Roberts et al., 2018).

Our approach to investigating the role the upper mantle plays in supporting topography along the margin has three parts. First, Schaeffer and Lebedev (2013)'s shear wave velocity model (SL2013sv) is converted to absolute velocities using their modified version of AK135 (Figure 9a-d). Secondly, absolute velocities are converted into temperature using the empirical approach of Priestley and McKenzie (2006) (Figure 9e-i). We note that their

methodology was developed using their own tomography so applying their parametrization to a different model (e.g. SL2013sv) might be problematic. We therefore also calculated temperatures using the mineral physics parametrization of Goes et al. (2012) with anelastic velocity correction (see e.g. Lodhia et al., 2018). Finally, these temperatures are used to perform a simple calculation to estimate isostatic support from upper mantle thermal anomalies. Calculated subsidence (or uplift) U, is a function of temperature dependent density such that

$$U = \frac{h\alpha\overline{T}}{1 - \alpha T_\circ}, \tag{11}$$

where h is thickness of the anomalously hot or cool layer, α is thermal expansivity, $\overline{T}$ is average excess temperature, $T_\circ$ is background temperature, which we set to 1333 ± 30°C (e.g. Rudge et al., 2008). The calculated topographic support from average excess thermal anomalies between 125–200 km depth is shown in Figures 9k and 10a for a background temperature of 1330°C. The transect in Figure 10 includes the Southeast Georgia Embayment, the Baltimore Canyon Trough and Georges Bank, and is shown alongside bathymetry and shear wave velocity anomalies. Maximum calculated subsidence along this transect is ~ 600 m centered on the Baltimore Canyon Trough. The pattern of sub-plate positive and negative support calculated by converting shear wave models into temperature is broadly consistent with the pattern of dynamic support estimated from ocean age-depth measurements, and with Neogene water-loaded subsidence of wells along the margin (Figure 9l; Hoggard et al., 2017; see also Steinberger et al., 2017).

5.3. Implications for eustasy

Eustatic sea level estimates are often calculated at supposedly tectonically stable passive margins (e.g. Vail et al., 1977; Miller et al., 2005). It is now generally accepted that dynamic topography can generate lithospheric vertical motions on space and time scales that overlap with estimates of eustasy (e.g. Hager et al., 1989; Hoggard et al., 2017). Most efforts to quantify the effect of sub-plate support for estimates of eustasy have focussed on results obtained by geodynamic models of mantle convection (e.g. Moucha et al., 2008; Kominz

et al., 2016; Austermann et al., 2017). Instead, we show how geophysical and stratigraphic observations (e.g. gravity, seismic, backstripped wells) can be combined with tomographic models and simple isostatic calculations to constrain wavelengths and amplitudes of dynamic support at passive margins. Our results indicate that a cool upper mantle has drawn down a $\sim$ 1000 km long stretch of Eastern North America's passive margin by up to $\sim$ 600 m (in water-loaded space). Drawdown of the margin during the last $\sim$ 23 Ma has been centered close to the Baltimore Canyon Trough. We note that the wavelength of calculated drawdown is smaller than many geodynamic predictions. The cause of this discrepancy is probably partly because most geodynamic models do not include the shallow upper mantle in their calculations of mantle flow.

Given that the mantle has a Rayleigh number of $\sim$ 10^6–10^8, the vertical motions of passive margins are expected to be affected by dynamic uplift and drawdown on a range of spatial and temporal scales. Some of these scales are akin to long term sea level changes, complicating the interpretation of sea level curves derived from 'stable' continental margins ($O(10^1$–$10^2)$ m, $O(10^{-1}$–$10^2)$ Ma).

6. Conclusions

Backstripping of sixteen wells along the Atlantic margin of North America shows that Neogene water-loaded subsidence was up to $\sim$ 600 m in the Baltimore Canyon Trough. This subsidence history cannot be readily explained by post-rift thermal subsidence, post-rift stretching or flexure. In contrast, Neogene subsidence from Georges Bank and the Southeast Georgia Embayment can be explained by post-rift lithospheric cooling. Seismic lines in the Baltimore Canyon Trough and Georges Bank show thick ($\sim$ 1 km) and thin ($<$ 200 m) Neogene sequences, respectively. Progradational and aggradational Neogene clinoforms in the Baltimore Canyon Trough reflect rapid generation of accommodation space and subsequent filling between $\sim$ 20–0 Ma. The amplitude of subsidence and its spatial localisation rules out eustasy as the sole contributor to the generation of accommodation space. Correlation

with free-air gravity anomalies and shear wave tomography velocities indicate that temperature variations in the uppermost convecting mantle generated sufficient density anomalies to drawdown the New Jersey margin. The patterns of dynamic subsidence shown in this study are similar to observations of ocean age-depth measurements, and suggest that the Baltimore Canyon Trough has been drawn down by up to $\sim$ 600 m since $\sim$ 20 Ma. Given the convective vigour of the mantle, such observations are expected throughout the stratigraphic record. Upper mantle convection appears to play an important role in generating accommodation space along passive margins, which may incorrectly have been interpreted as a signal of eustasy in the past.

7. Acknowledgments

We thank P. Audet for providing his grid of elastic thicknesses, R. Bell, A. Lipp, S. Mitchell, and J. Quye-Sawyer for their help, and B. Steinberger and an anonymous person for their helpful reviews. Publicly available well data were downloaded from `https://www.ngdc.noaa.gov`. Seismic SEG-Y and PDF data are available at `https://walrus.wr.usgs.gov/NAMSS` and `https://cmgds.marine.usgs.gov`. GRACE gravity data are available from `https://grace.jpl.nasa.gov`. ETOPO1 data are available to download from `https://catalog.data.gov/dataset/etopo1-1-arc-minute-global-relief-model`.

8. Bibliography

Allen, P. A., Allen, J. R., 2005. Basin Analysis. In: Basin Analysis - Principles and Analysis, 2nd Edition. Blackwell Science Ltd, Ch. 3, p. 73.

Athy, L., 1930. Density, porosity, and compaction of sedimentary rocks. Bulletin of the American Association of Petroleum Geologists 14 (1), 1–24.

Audet, P., 2014. Toward mapping the effective elastic thickness of planetary lithospheres from a spherical wavelet analysis of gravity and topography. Physics of the Earth and Planetary Interiors 226, 48–82.

Audet, P., Bürgmann, R., 2011. Toward mapping the effective elastic thickness of planetary lithospheres from a spherical wavelet analysis of gravity and topography. Nature Geosciences 4, 48–82.

Austermann, J., Mitrovica, J. X., Huybers, P., Rovere, A., 2017. Detection of a dynamic topography signal in last interglacial sea-level records. Science Advances 3 (7).

Benson, R. N., Doyle, R. G., 1988. Chapter 5: Early Mesozoic rift basins and the development of the United States middle Atlantic continental margin. In: W. Manspeizer (ed.) Triassic-Jurassic rifting: continental breakup and the origin of the Atlantic Ocean and passive margins, Developments in Geotectonics 22, 99–127.

Browning, J. V., Miller, K. G., McLaughlin, P. P., Kominz, M. A., Sugarman, P. J., Monteverde, D., Feigenson, M. D., Hernández, J. C., 2006. Quantification of the effects of eustasy, subsidence, and sediment supply on Miocene sequences, mid-Atlantic margin of the United States. Bulletin of the Geological Society of America 118 (5-6), 567–588.

Cloetingh, S., Gradstein, F. M., Kooi, H., Grant, A. C., Kaminski, M., 1990. Plate reorganization: a cause of rapid late Neogene subsidence and sedimentation around the North Atlantic? Journal of the Geological Society 147 (3), 495–506.

Cloetingh, S., Haq, B. U., 2015. Inherited landscapes and sea level change. Science 347 (6220).

Clouzet, P., Masson, Y., Romanowicz, B., 2018. Box tomography: first application to the imaging of upper-mantle shear velocity and radial anisotropy structure beneath the north american continent. Geophysical Journal International 213 (3), 1849–1875.

Colli, L., Ghelichkhan, S., Bunge, H.-P., 2016. On the ratio of dynamic topography and gravity anomalies in a dynamic Earth. Geophysical Research Letters 43 (6), 2510–2516.

Cornet, B., Olsen, P. E., 1985. A summary of the biostratigraphy of the Newark Supergroup of Eastern North America with comments on Early Mesozoic provinciality. III Congreso Latinoamericano de Paleontologia. Mexico. Simposio sobre floras del Triassico Tardio, su fitogeografia y paleoecologia. Memoria., 61–81.

Courtillot, V., Davaille, A., Besse, J., Stock, J., 2003. Three distinct types of hotspots in the Earth's mantle. Earth and Planetary Science Letters 205 (3), 295–308.

Cousminer, H. L., 1983. Late Triassic dinoflagellate cycts date Georges Bank deep marine sediments as Rhaeto-Norian. Proc., Am. Assoc. Stratigr. Palynol. 2.

Cousminer, H. L., Steinkraus, W. E., 1988. COST G-2 Well: Biostratigraphy and implications for the origin of the Atlantic passive margin. In: Manspeizer (ed.) Triassic-Jurassic rifting: continental breakup and the origin of the Atlantic Ocean and passive margins, Developments in Geotectonics 22, 167–184.

Crosby, A. G., McKenzie, D., Sclater, J. G., 2006. The relationship between depth, age and gravity in the oceans. Geophysical Journal International 166 (2), 553–573.

Czarnota, K., Roberts, G. G., White, N. J., Fishwick, S., 2014. Spatial and temporal patterns of Australian dynamic topography from river profile modeling. Journal of Geophysical Research: Solid Earth 119 (2), 1384–1424.

Durand, S., Debayle, E., Ricard, Y., Zarioli, C., Lambotte, S., 2017. Confirmation of a change in the global shear velocity pattern at around 1,000 km depth. Geophysical Journal International 211 (3), 1628–1639.

497 Flament, N., Gurnis, M., Müller, R. D., 2013. A review of observations and models of
498 dynamic topography. Lithosphere 5 (2), 189–210.

499 Forte, A. M., Mitrovica, J. X., Moucha, R., Simmons, N. A., Grand, S. P., 2007. Descent of
500 the ancient Farallon slab drives localized mantle flow below the New Madrid seismic zone.
501 Geophysical Research Letters 34 (4).

502 French, S. W., Romanowicz, B. A., 2014. Whole-mantle radially anisotropic shear velocity
503 structure from spectral-element waveform tomography. Geophysical Journal International
504 199 (3), 1303–1327.

505 Goes, S., Armitage, J., Harmon, N., Smith, H., Huismans, R., 2012. Low seismic veloci-
506 ties below mid-ocean ridges: Attenuation versus melt retention. Journal of Geophysical
507 Research: Solid Earth 117 (B12).

508 Greene, J., Tominaga, M., Miller, N. C., Hutchinson, D., Karl, M. R., 2017. Refining the for-
509 mation and early evolution of the Eastern North American Margin: New insights from mul-
510 tiscale magnetic anomaly analyses. Journal of Geophysical Research: Solid Earth 122(11),
511 8724–8748.

512 Greenlee, S. M., Devlin, W. J., Miller, K., 11 1992. Integrated sequence stratigraphy of
513 Neogene deposits, New Jersey continental shelf and slope: Comparison with the Exxon
514 model. Geological Society of America Bulletin 104, 1403–1411.

515 Greenlee, S. M., Schroeder, F. W., Vail, P. R., 01 1988. Seismic stratigraphic and geohistory
516 analysis of Tertiary strata from the continental shelf off New Jersey; Calculation of eustatic
517 fluctuations from stratigraphic data. In: The Atlantic Continental Margin. Geological
518 Society of America.

519 Grow, J., Klitgord, K., Schlee, J., 1988. Structure and evolution of Baltimore Canyon Trough.
520 The Atlantic Continental Margin, U.S. 1, 269–290.

Grow, J. A., Hutchinson, D. R., Klitgord, K. D., Dillon, W. P., Schlee, J. S., 1983. Representative multichannel seismic profiles over the US Atlantic margin. Seismic expression of structural styles: AAPG Studies in Geology 15 (1-2).

Hager, B. H., Richards, M. A., O'Nions, R. K., Clayton, R., Parsons, B., 1989. Long-wavelength variations in Earth's geoid: Physical models and dynamical implications. Philosophical Transactions of the Royal Society of London. Series A, Mathematical and Physical Sciences 328 (1599), 309–327.

Hartley, R. A., Roberts, G. G., White, N., Richardson, C., 2011. Transient convective uplift of an ancient buried landscape. Nature Geosciences 4 (8), 562–565.

Hoggard, M. J., Winterbourne, J., Czarnota, K., White, N., 2017. Oceanic residual depth measurements, the plate cooling model, and global dynamic topography. Journal of Geophysical Research: Solid Earth.

Jarvis, G. T., McKenzie, D. P., 1980. Sedimentary basin formation with finite extension rates. Earth and Planetary Science Letters 48, 42–52.

Kominz, M. A., Browning, J. V., Miller, K. G., Sugarman, P. J., Mizintseva, S., Scotese, C. R., 2008. Late Cretaceous to Miocene sea-level estimates from the New Jersey and Delaware coastal plain coreholes: An error analysis. Basin Research 20 (2), 211–226.

Kominz, M. A., Miller, K. G., Browning, J. V., 1998. Long-term and short-term global Cenozoic sea-level estimates. Geology 26 (4), 311–314.

Kominz, M. A., Miller, K. G., Browning, J. V., Katz, M. E., Mountain, G. S., 2016. Miocene relative sea level on the New Jersey shallow continental shelf and coastal plain derived from one-dimensional backstripping: A case for both eustasy and epeirogeny. Geosphere 12 (5), 1437–1456.

Lambeck, K., Chappell, J., 1988. Sea Level Change through the Last Glacial Cycle. Science 292 ((5517)), 679–686.

Le Pichon, X., Sibuet, J., 1981. Passive margins: A model of formation. Journal of Geophysical Research 86 (B5), 3708–3720.

Lithgow-Bertelloni, C., Silver, P. G., 1998. Dynamic topography, plate driving forces and the African superswell. Nature 395 (September), 345–348.

Liu, L., 2015. The ups and downs of North America: Evaluating the role of mantle dynamic topography since the Mesozoic. Reviews of Geophysics 53 (3), 1022–1049.

Lodhia, B. H., Roberts, G. G., Fraser, A. J., Fishwick, S., Goes, S., Jarvis, J., 2018. Continental margin subsidence from shallow mantle convection: Example from West Africa. Earth and Planetary Science Letters 481, 350–361.

Manspeizer, W., 1988. Triassic-Jurassic rifting: continental breakup and the origin of the Atlantic Ocean and passive margins. Developments in Geotectonics 22.

McKenzie, D., 1978. Some remarks on the development of sedimentary basins. Earth and Planetary Science Letters 40 (1), 25–32.

McKenzie, D., 2010. The influence of dynamically supported topography on estimates of Te. Earth and Planetary Science Letters 295, 127–138.

McNab, F., Ball, P. W., Hoggard, M. J., White, N. J., 2018. Neogene uplift and magmatism of Anatolia: insights from drainage analysis and basaltic geochemistry. Geochem. Geophys. Geosyst.

Miller, K. G., Browning, J. V., Mountain, G. S., Bassetti, M. A., Monteverde, D., Katz, M. E., Inwood, J., Lofi, J., Proust, J. N., 2013. Sequence boundaries are impedance contrasts: Core-seismic-log integration of Oligocene-Miocene sequences, New Jersey shallow shelf. Geosphere 9 (5), 1257–1285.

Miller, K. G., Kominz, M. A., Browning, J. V., Wright, J. D., Mountain, G. S., Katz, M. E., Sugarman, P. J., Cramer, B. S., Christie-Blick, N., Pekar, S. F., 2005. The Phanerozoic record of global sea-level change. Science 310 (5752), 1293–1298.

571 Miller, K. G., Sugarman, P. J., Browning, J. V., McLaughlin, P. P., Benson, R. N.,
572 Hernández, J. C., Ramsey, K. W., Baxter, S. J., Feigenson, M. D., Aubry, M.-P., Mon-
573 teverde, D. H., Cramer, B. S., Katz, M. E., McKenna, T. E., Strohmeier, S. A., Pekar,
574 S. F., Uptegrove, J., Cobbs, G., Cobbs III, G., Curtin, S. E., 2003. Bethany Beach Site.
575 In: Proceedings of the Ocean Drilling Program, Initial Reports. Vol. 174AX (Suppl). pp.
576 1–85.

577 Monteverde, D. H., Mountain, G. S., Miller, K. G., 2008. Early Miocene sequence develop-
578 ment across the New Jersey margin. Basin Research 20 (2), 249–267.

579 Moucha, R., Forte, A. M., Mitrovica, J. X., Rowley, D. B., Quéré, S., Simmons, N. A.,
580 Grand, S. P., 2008. Dynamic topography and long-term sea-level variations: There is no
581 such thing as a stable continental platform. Earth and Planetary Science Letters 271 (1-4),
582 101–108.

583 Moulik, P., Ekstrom, G., 2014. An anisotropic shear velocity model of the Earth's mantle
584 using normal modes, body waves, surface waves and long-period waveforms. Geophysical
585 Journal International 199 (3), 1713–1738.

586 Müller, R. D., Hassan, R., Gurnis, M., Flament, N., Williams, S. E., 2018. Dynamic topogra-
587 phy of passive continental margins and their hinterlands since the Cretaceous. Gondwana
588 Research 53, 225–251.

589 Müller, R. D., Sdrolias, M., Gaina, C., Steinberger, B., Heine, C., 2008. Long-Term Sea-Level
590 Fluctuations. Science 319 (March), 1357–1363.

591 Pazzaglia, F. J., Gardner, W., 1994. Late Cenozoic flexural deformation of the middle U.S.
592 Atlantic passive margin. Journal of Geophysical Research 99 (B6), 12143–12157.

593 Poag, C. W., Sevon, W., 1989. A record of Appalachian denudation in postrift Mesozoic and
594 Cenozoic sedimentary deposits of the U.S. Middle Atlantic continental margin. Geomor-
595 phology 2 (1989), 119–157.

Posamentier, H. W., Jervey, M. T., Vail, P. R., 1988. Eustatic controls on clastic deposition iconceptual framework. In: Sea-Level Changes: An Integrated Approach. No. 42. pp. 125–154.

Priestley, K., McKenzie, D., 2006. The thermal structure of the lithosphere from shear wave velocities. Earth and Planetary Science Letters 244 (1), 285–301.

Ritsema, J., Deuss, A., Van Heijst, H. J., Woodhouse, J. H., 2011. S40RTS: a degree-40 shear-velocity model for the mantle from new Rayleigh wave dispersion, teleseismic travel-time and normal-mode splitting function measurements. Geophysical Journal International 184 (3), 1223–1236.

Roberts, G. G., White, N., Hoggard, M. J., Ball, P. W., Meenan, C., 2018. A Neogene history of mantle convective support beneath Borneo. Earth and Planetary Science Letters 496, 142–158.

Roberts, G. G., White, N. J., Martin-Brandis, G. L., Crosby, A. G., 2012. An uplift history of the Colorado Plateau and its surroundings from inverse modeling of longitudinal river profiles. Tectonics 31 (4).

Rovere, A., Raymo, M. E., Mitrovica, J. X., Hearty, P. J., Leary, M. J. O., Inglis, J. D., 2014. The Mid-Pliocene sea-level conundrum: Glacial isostasy , eustasy and dynamic topography. Earth and Planetary Science Letters 387 (2014), 27–33.

Rowley, D., Forte, A. M., Moucha, R., Mitrovica, J. X., Simmons, N., Grand, S. P., 2013. Dynamic Topography Change of the Eastern United States since 3 Million Years ago. Science 340, 1560–1563.

Rudge, J. F., Champion, M. E. S., White, N., McKenzie, D., Lovell, B., 2008. A plume model of transient diachronous uplift at the Earth's surface. Earth and Planetary Science Letters 267 (1), 146–160.

Schaeffer, A. J., Lebedev, S., 2013. Global shear speed structure of the upper mantle and transition zone. Geophysical Journal International 194 (1), 417–449.

Scholle, P., Mattick, R. E., Rhodehamel, E. C., Poag, C. W., Valentine, P. C., Scott, R. A., Robbins, E. I., Claypool, G. E., Lubeck, C. M., Baysinger, J. P., Ging, T. G., Taylor, D. J., Bayer, K. C., 1977. Geological Studies on the COST No. B-2 Well, U.S. Mid-Atlantic Outer Continental Shelf Area. Tech. rep., United States Department of the Interior Geological Survey.

Seidemann, D. E., Masterson, W. D., Dowling, M. P., Turekian, K. K., 1984. K-Ar dates and 40Ar/39Ar age spectra for Mesozoic basalt flows of the Hartford Basin, Connecticut, and the Newark Basin, New Jersey. Geological Society of America Bulletin 95 (5), 594–598.

Sheridan, R. E., Musser, D., Glover III, L., Talwani, M., Ewing, J. I., Holbrook, W. S., Purdy, G. M., Hawman, R., Smithson, S., 1993. Deep seismic reflection data of EDGE US mid-Atlantic continental-margin experiment: Implications for Appalachian sutures and Mesozoic rifting and magmatic underplating. Geology 21 (6), 563–567.

Smith, M. A., Amato, R. V., Furbush, M. A., Pert, D. M., Nelsom, M. E., Hendrix, J. S., Tamm, L. C., Wood Jr, G., Shaw, D. R., 1976. Geological and Operational Summary, COST No. B-2 Well, Baltimore Canyon Trough Area, Mid-Atlantic OCS. Tech. rep., United States Department of the Interior Geological Survey.

Spasojević, S., Gurnis, M., 2012. Sea level and vertical motion of continents from dynamic earth models since the late cretaceous. AAPG Bulletin 96 (11), 2037–2064.

Spasojević, S., Liu, L., Gurnis, M., Müller, R. D., 2008. The case for dynamic subsidence of the U.S. east coast since the Eocene. Geophysical Research Letters 35 (8), 1–6.

Steckler, M. S., Watts, A. B., 1978. Subsidence of the Atlantic-type continental margin off New York. Earth and Planetary Science Letters 41 (13), 1–13.

Steinberger, B., Conrad, C. P., Tutu, A. O., Hoggard, M. J., 2017. On the amplitude of dynamic topography at spherical harmonic degree two. Tectonophysics.

Sutter, J. F., 1988. Innovative approaches to the dating of igneous events in the early Mesozoic basins of the eastern United States. in Froelich, A.J., and Robinson, G.R., eds., Studies of the early Mesozoic basins of the eastern United States: U.S. Geological Survey Bulletin 1776, 194–200.

Tapley, B., Ries, J., Bettadpur, S., Chambers, D., Cheng, M., Condi, F., Gunter, B., Kang, Z., Nagel, P., Pastor, R., Pekker, T., Poole, S., Wang, F., Nov 2005. GGM02 – An improved Earth gravity field model from GRACE. Journal of Geodesy 79 (8), 467–478.

Turcotte, D. L., Schubert, G., 2002. Geodynamics, 2nd Edition. Cambridge University Press.

Vail, P. R., Mitchum, R. M., Thompson, S., 1977. Seismic Stratigraphy and Global Changes of Sea Level, Part 4: Global Cycles of Relative Changes of Sea Level. 1. In: Payton, C. E. (Ed.), Seismic stratigraphy - Applications to Hydrocarbon Exploration. Ch. 4.

Van Sickel, W., Kominz, M. A., Miller, K. G., Browning, J. V., 2004. Late Cretaceous and Cenozoic sea-level estimates: backstripping analysis of borehole data, onshore New Jersey. Basin Research 16 (4), 451–465.

Vanderaveroet, P., 2000. Miocene to Pleistocene clay mineral sedimentation on the New Jersey shelf. Oceanologica Acta 23 (1), 25–36.

Watts, A. B., Ryan, W. B., 1976. Flexure of the lithosphere and continental margin basins. Developments in Geotectonics 12 (C), 25–44.

Watts, A. B., Thorne, J., 1984. Tectonics, global changes in sea level and their relationship to stratigraphical sequences at the US Atlantic continental margin. Marine and Petroleum Geology 1 (4), 319–339.

Weems, R. E., Olsen, P. E., 1997. Synthesis and revision of groups within the Newark Supergroup, eastern North America. Bull. Geol. Soc. Am. 109, 195–209.

White, N., 1994. An inverse method for determining lithospheric strain rate variation on geological timescales. Earth and Planetary Science Letters 122 (3), 351 – 371.

671 Wyllie, M. R. J., Gregory, A. R., Gardner, L. W., 1956. Elastic wave velocities in heteroge-
672 neous and porous media. Geophysics 21 (1), 41–70.

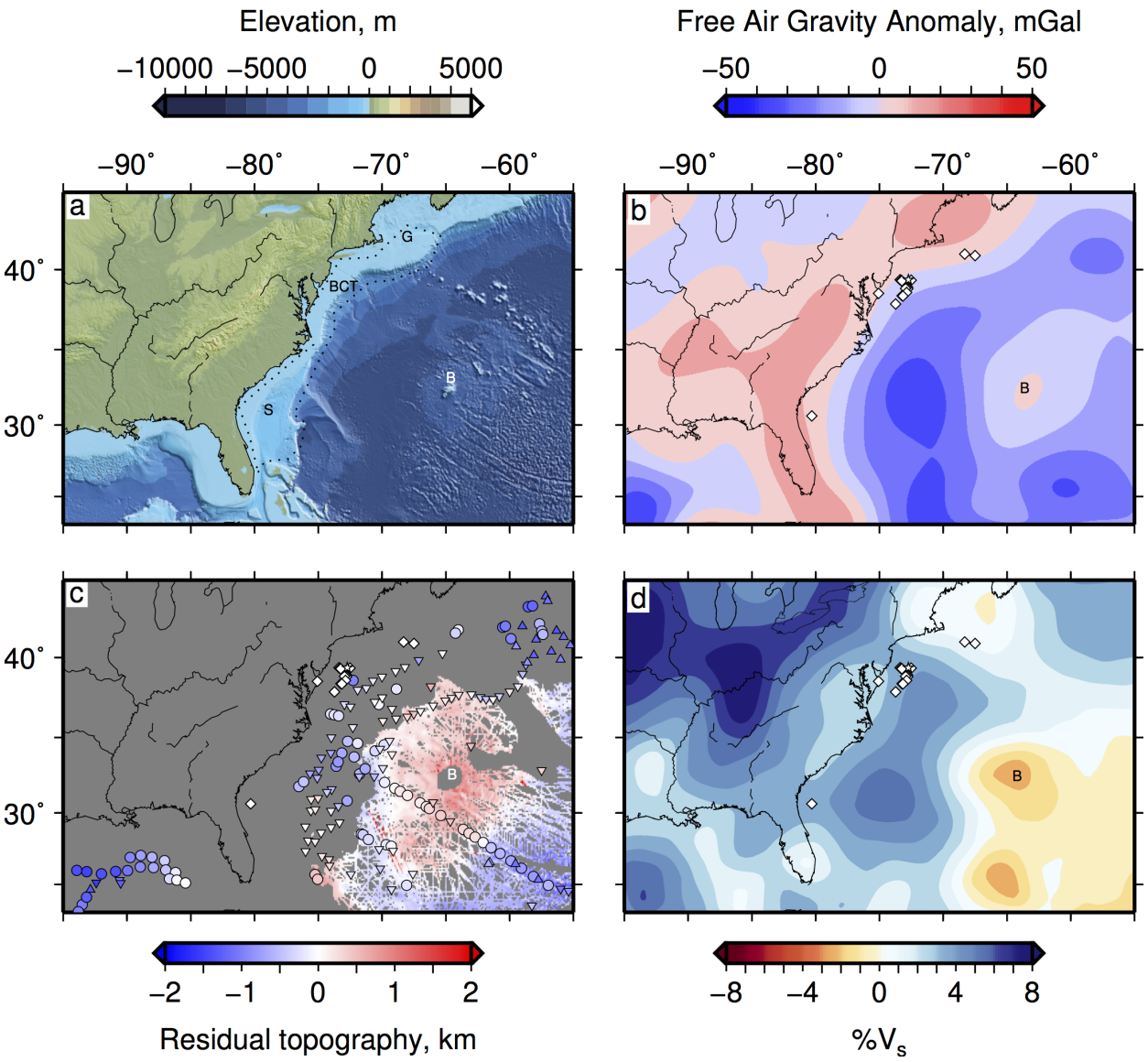


Figure 1: **Eastern North America and Atlantic Ocean.** (a) Topography and bathymetry of the Eastern North American passive margin (ETOPO1 dataset). Dotted line indicates extent of seismic data. G = Georges Bank, BCT = Baltimore Canyon Trough, S = Southeast Georgia Embayment, B = Bermuda Rise. (b) Free air gravity anomalies from the GRACE dataset, filtered to remove wavelengths $\lesssim$ 800 km. Diamonds = wells backstripped in this study. (c) Geoid-corrected residual ocean-age depths in 1° bins (Hoggard et al., 2017). Circles represent measurements with sedimentary and crustal corrections applied. Up/down pointing triangles = lower/upper limits for which only a sedimentary correction has been applied. Filigree = residual ocean-age depth estimates from ship track data. (d) Slice through SL2013sv shear wave tomographic model at 125 km depth (Schaeffer and Lebedev, 2013). Note that free-air gravity anomalies and residual topography of the Baltimore Canyon Trough and its surroundings are negative, and the region sits atop fast upper mantle shear wave velocity anomalies.

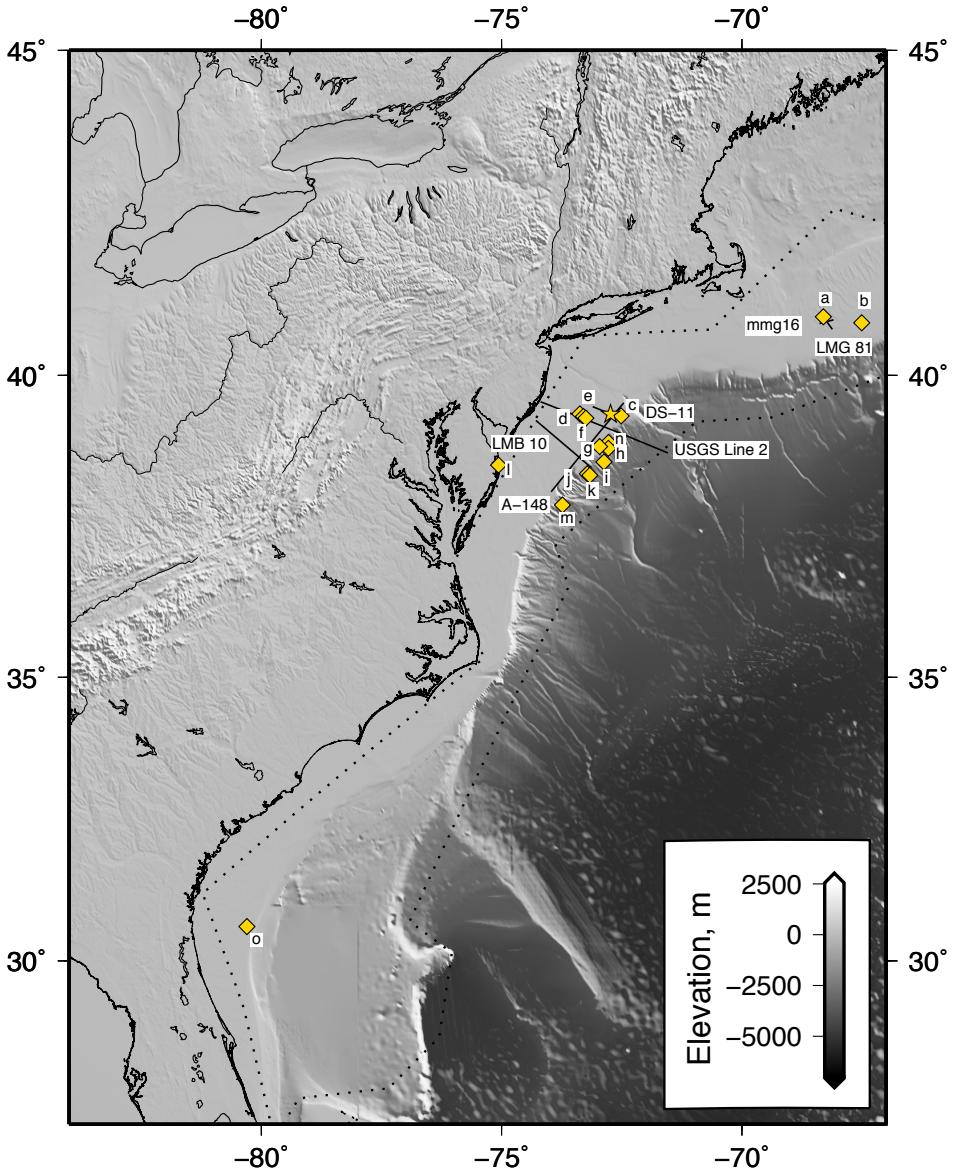


Figure 2: **Passive margin of eastern North America from Miami to Maine.** Labelled gold diamonds = backstripped wells: a = COST G-1, b = COST G-2, c = Texaco 642-1, d = IODP 313 M27, e = IODP 313 M28, f = IODP 313 M29, g = Murphy 106-1, h = DSDP 612, i = Shell 372-1, j = Shell 586-1, k = Shell 587-1, l = Bethany Beach, m = Shell 93-1, n = COST B-3, o = COST GE-1. Gold star = COST B-2. Dotted line = extent of available seismic data; solid black lines = seismic reflection data shown in Figure 6 and Supplementary Material.

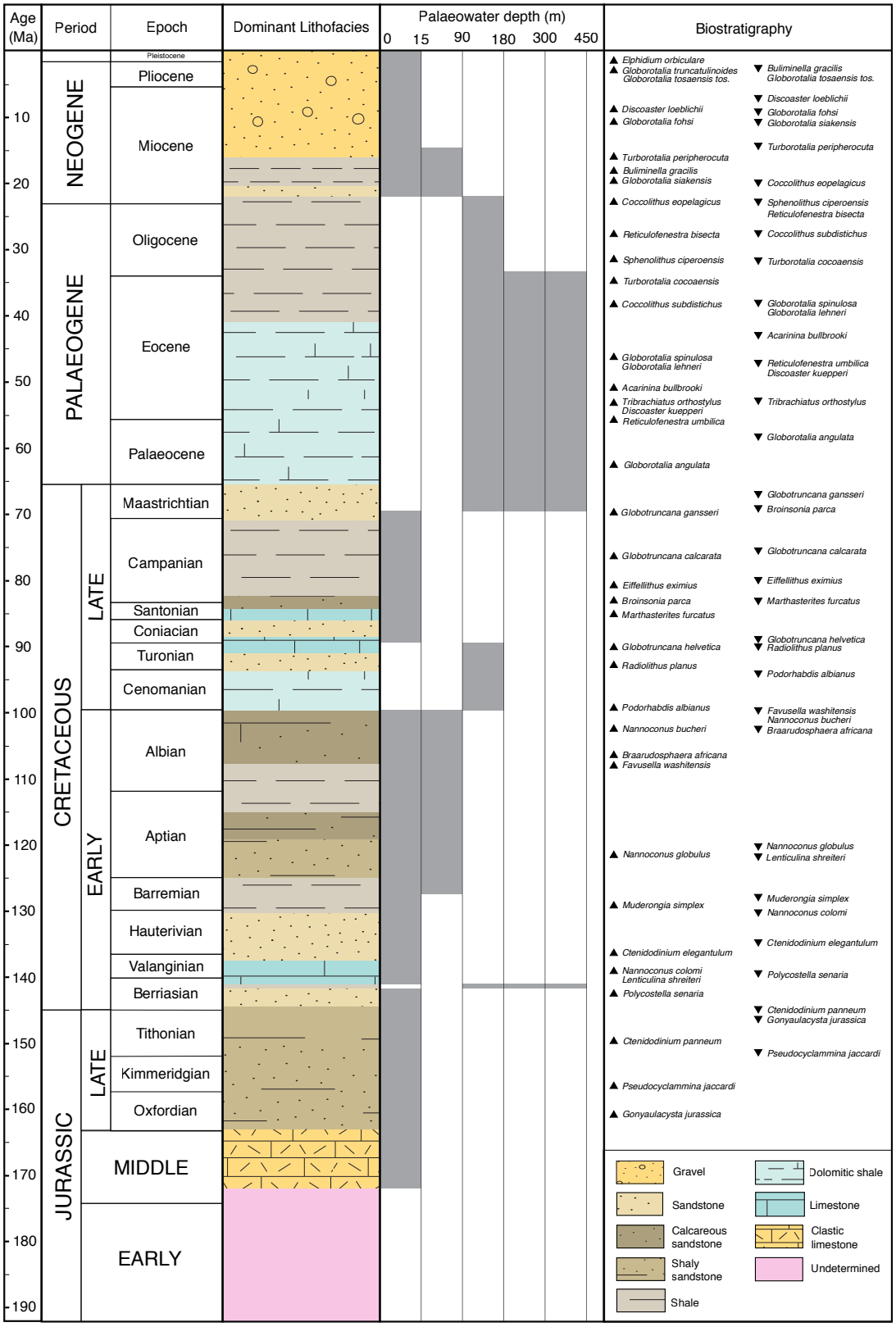

Age (Ma)
Period
Epoch
Dominant Lithofacies
Palaeowater depth (m)
0 15 90 180 300 450
Biostratigraphy
Pleistocene
Pliocene
Miocene
Oligocene
Eocene
Palaeocene
Maastrichtian
Campanian
Santonian
Coniacian
Turonian
Cenomanian
Albian
Aptian
Barremian
Hauterivian
Valanginian
Berriasian
Tithonian
Kimmeridgian
Oxfordian
MIDDLE
EARLY
NEOGENE
PALAEOGENE
CRETACEOUS
JURASSIC
LATE
EARLY
10
20
30
40
50
60
70
80
90
100
110
120
130
140
150
160
170
180
190
▲ Elphidium orbiculare
▲ Globorotalia truncatulinoides
Globorotalia tosaensis tos.
▲ Discoaster loeblichii
▲ Globorotalia fohsi
▲ Turborotalia peripherocuta
▲ Buliminella gracilis
▲ Globorotalia siakensis
▲ Coccolithus eopelagicus
▲ Reticulofenestra bisecta
▲ Sphenolithus ciperoensis
▲ Turborotalia cocoaensis
▲ Coccolithus subdistichus
▲ Globorotalia spinulosa
Globorotalia lehneri
▲ Acarinina bullbrooki
▲ Tribrachiatus orthostylus
Discoaster kuepperi
▲ Reticulofenestra umbilica
▲ Globorotalia angulata
▲ Globotruncana gansseri
▲ Globotruncana calcarata
▲ Eiffellithus eximius
▲ Broinsonia parca
▲ Marthasterites furcatus
▲ Globotruncana helvetica
▲ Radiolithus planus
▲ Podorhabdis albianus
▲ Nannoconus bucheri
▲ Braarudosphaera africana
▲ Favusella washitensis
▲ Nannoconus globulus
▲ Muderongia simplex
▲ Ctenidodinium elegantulum
▲ Nannoconus colomi
Lenticulina shreiteri
▲ Polycostella senaria
▲ Ctenidodinium panneum
▲ Pseudocyclammina jaccardi
▲ Gonyaulacysta jurassica
▼ Buliminella gracilis
Globorotalia tosaensis tos.
▼ Discoaster loeblichii
▼ Globorotalia fohsi
▼ Globorotalia siakensis
▼ Turborotalia peripherocuta
▼ Coccolithus eopelagicus
▼ Sphenolithus ciperoensis
Reticulofenestra bisecta
▼ Coccolithus subdistichus
▼ Turborotalia cocoaensis
▼ Globorotalia spinulosa
Globorotalia lehneri
▼ Acarinina bullbrooki
▼ Reticulofenestra umbilica
Discoaster kuepperi
▼ Tribrachiatus orthostylus
▼ Globorotalia angulata
▼ Globotruncana gansseri
▼ Broinsonia parca
▼ Globotruncana calcarata
▼ Eiffellithus eximius
▼ Marthasterites furcatus
▼ Globotruncana helvetica
▼ Radiolithus planus
▼ Podorhabdis albianus
▼ Favusella washitensis
Nannoconus bucheri
▼ Braarudosphaera africana
▼ Nannoconus globulus
▼ Lenticulina shreiteri
▼ Muderongia simplex
▼ Nannoconus colomi
▼ Ctenidodinium elegantulum
▼ Polycostella senaria
▼ Ctenidodinium panneum
▼ Gonyaulacysta jurassica
▼ Pseudocyclammina jaccardi
Gravel
Sandstone
Calcareous sandstone
Shaly sandstone
Shale
Dolomitic shale
Limestone
Clastic limestone
Undetermined

Figure 3: **Chronostratigraphy of the Baltimore Canyon Trough.** Lithofacies are synthesised from wells across the Baltimore Canyon Trough. Palaeowater depths were extracted from well reports, and were interpreted from benthic fauna and environmental settings; gray band = palaeowater depth uncertainty (Smith et al., 1976; Scholle et al., 1977). Right panel shows first (upward pointing triangle) and last (downward pointing triangle) appearances of common and dominant species in the Baltimore Canyon Trough used to constrain age of stratigraphy.

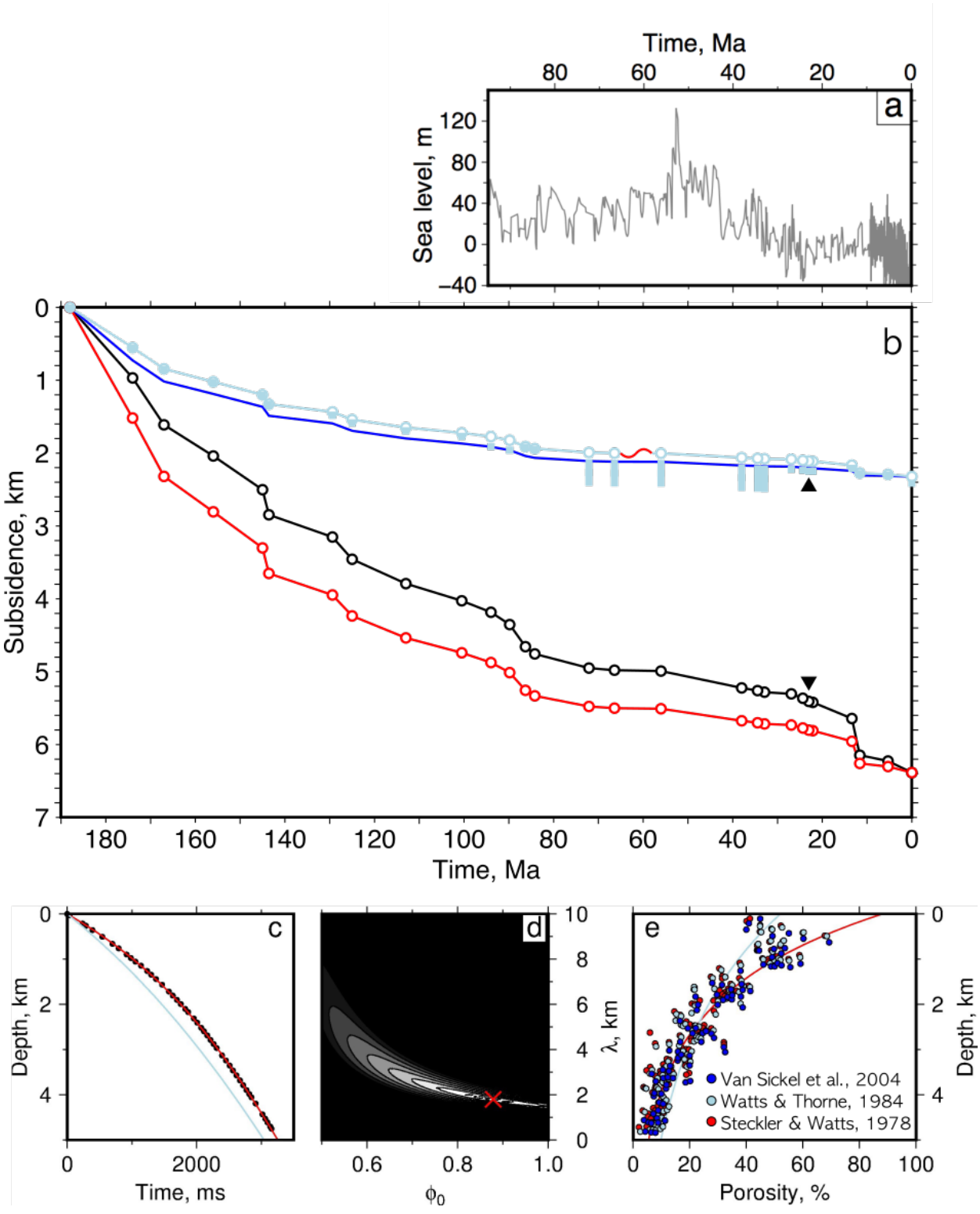

Time, Ma
80
60
40
20
0
a
Sea level, m
120
80
40
0
−40
b
Subsidence, km
0
1
2
3
4
5
6
7
180
160
140
120
100
80
60
40
20
0
Time, Ma
c
Depth, km
0
2
4
0
2000
Time, ms
d
10
8
6
4
2
0
0.6
0.8
1.0
ϕ_0
λ, km
e
Depth, km
0
2
4
0
20
40
60
80
100
Porosity, %
Van Sickel et al., 2004
Watts & Thorne, 1984
Steckler & Watts, 1978

Figure 4: **History of New Jersey subsidence.** (a) Eustasy calculated from reduced subsidence history of COST B-2 well, New Jersey margin, from 98.4 to 9.25 Ma and oxygen isotopes from 9.25 to 0 Ma (Miller et al., 2005). (b) Subsidence at COST B-2 well from stratigraphy described in the well reports: black = backstripped burial curve; red = decompacted subsidence; light blue = decompacted, water-loaded subsidence. Dark blue rectangles = decompacted, water-loaded subsidence, with added palaeowater depth uncertainties, obtained from well reports (see e.g., Figure 3). Yellow = water-loaded subsidence curve generated using Watts and Thorne (1984)'s compaction parameterization (see panel e). Arrow = onset of anomalous Neogene subsidence. (c) Black circles = time-depth measurements in the COST B-2 well from check shots; red curve = best-fitting theoretical time-depth relationship for compaction parameters indicated by red cross in panel d. Yellow curve = time-depth relationship for initial porosity, $\phi_\circ = 0.52$, and compaction wavelength, $\lambda = 3$ km (Watts and Thorne, 1984). (d) Color scale = misfit between observed and calculated time-depth relationship for COST B-2 well (panel c). Parameter sweep was performed for range of $\phi_\circ$ and λ values. Red cross = best-fitting values used to generate red curve in panel c. (e) Red curve = best-fitting porosity-depth relationship calculated from check shot data. Colored circles = measured porosities as a function of depth (Steckler and Watts, 1978; Watts and Thorne, 1984; Van Sickel et al., 2004). Yellow curve = porosity as a function of depth calculated using Watts and Thorne (1984)'s parametrization.

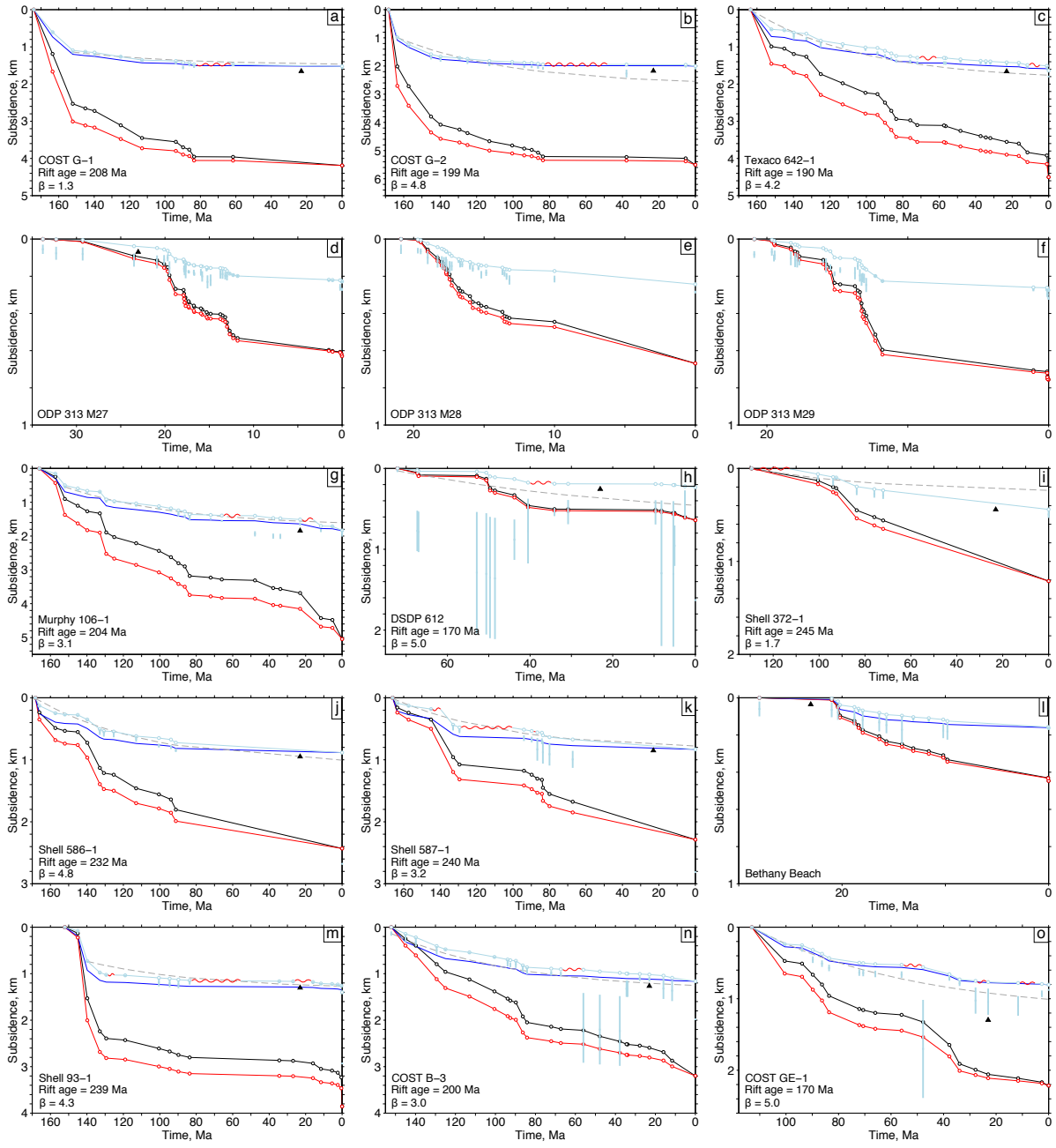


Figure 5: **History of passive margin subsidence**. (a-o) Subsidence curves for wells on the Eastern North American passive margin (see Figure 2 for location). Wavy red curves represent unconformities. Annotation is same as for Figure 4b. Black/red/light blue curves = burial/decompacted/water-loaded subsidence curves. Blue rectangles = water-loaded (tectonic) subsidence curves with added paleowater depth uncertainties. Black triangles = onset of Neogene Period. Dashed lines = best-fitting thermal subsidence history calculated assuming instantaneous rifting. Best-fitting thermal subsidence curves are shown for wells with accurately matched pre-Neogene stratigraphy. Note that expected Neogene thermal subsidence is $O(10)$ m.

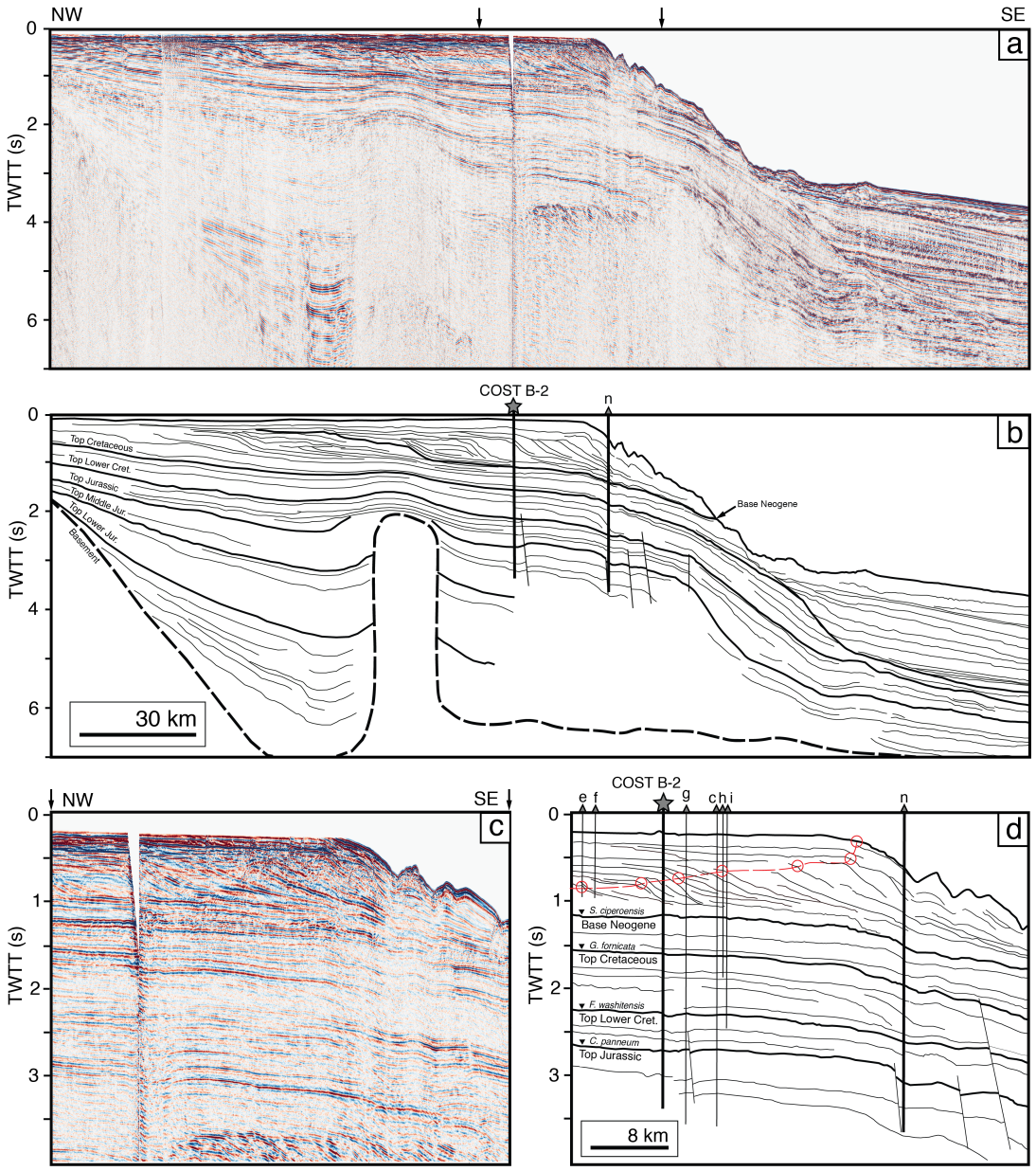


Figure 6: **Stratigraphy of the New Jersey margin.** (a) Seismic line USGS Line 2 (Figure 2). Arrows = extent of zoomed-in image shown in panels (c) and (d). (b) Interpreted stratigraphy. Annotated triangle, star and vertical lines = wells projected onto line (see Figure 2). Thick black curves = key stratigraphic horizons. Thin black curves are indicative of stratigraphic architecture. (c & d) Central portion of USGS Line 2 and interpreted stratigraphy. Annotated inverted triangles = last appearances of key biostratigraphic markers extracted from well reports (see e.g. Figure 3). Red circles and dashed curve = trajectory of clinoforms. Note $\sim$ 1 s of Neogene stratigraphy, which contains prograding and aggrading clinoforms. Labelled triangles, star and vertical lines = wells projected onto transect (see Figure 2).

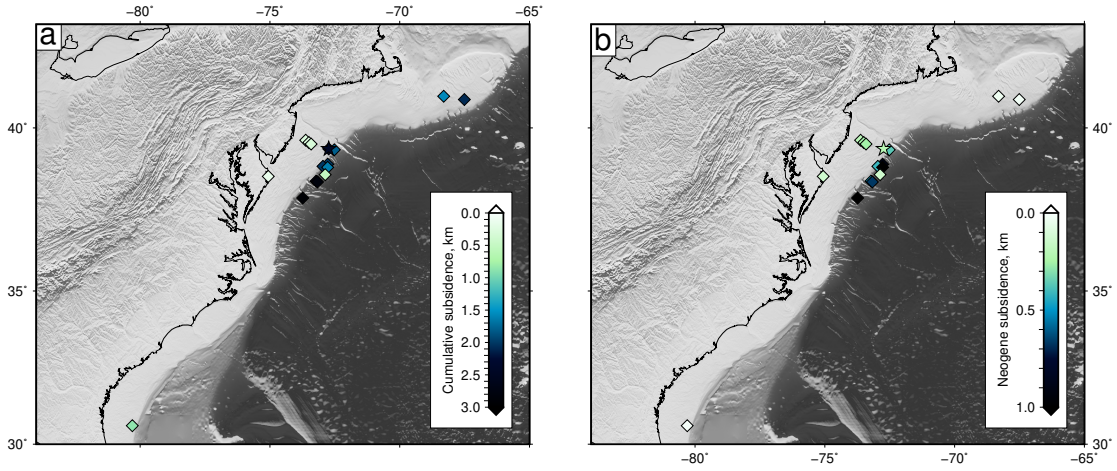
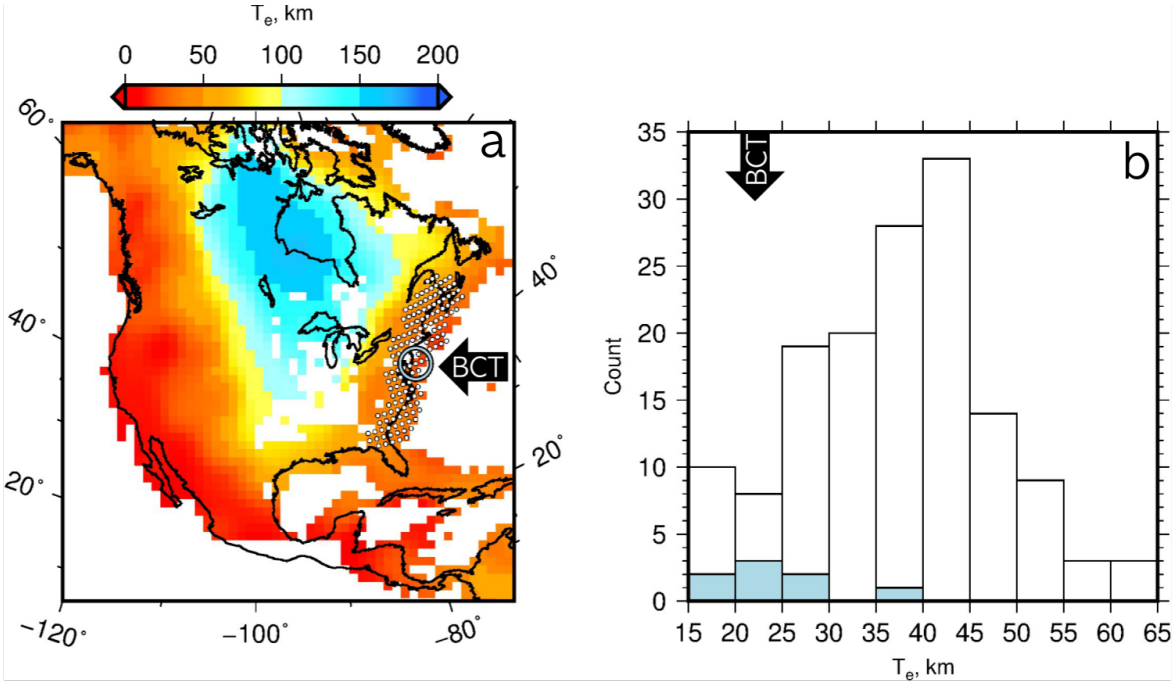


Figure 7: **Tectonic subsidence**. (a) Colored diamonds = cumulative water-loaded subsidence calculated by backstripping wells along Eastern North America's passive margin (Figures 2 & 5). (b) Neogene water-loaded subsidence. Note that wells without biostratigraphically constrained Neogene ages are not included in this synthesis (e.g. COST G-1, Shell 372-1). Highest Neogene subsidence is centered on the Baltimore Canyon Trough.


T_e, km
0
50
100
150
200
a
BCT
60°
40°
20°
−120°
−100°
−80°
b
BCT
Count
T_e, km
0
5
10
15
20
25
30
35
15
20
25
30
35
40
45
50
55
60
65

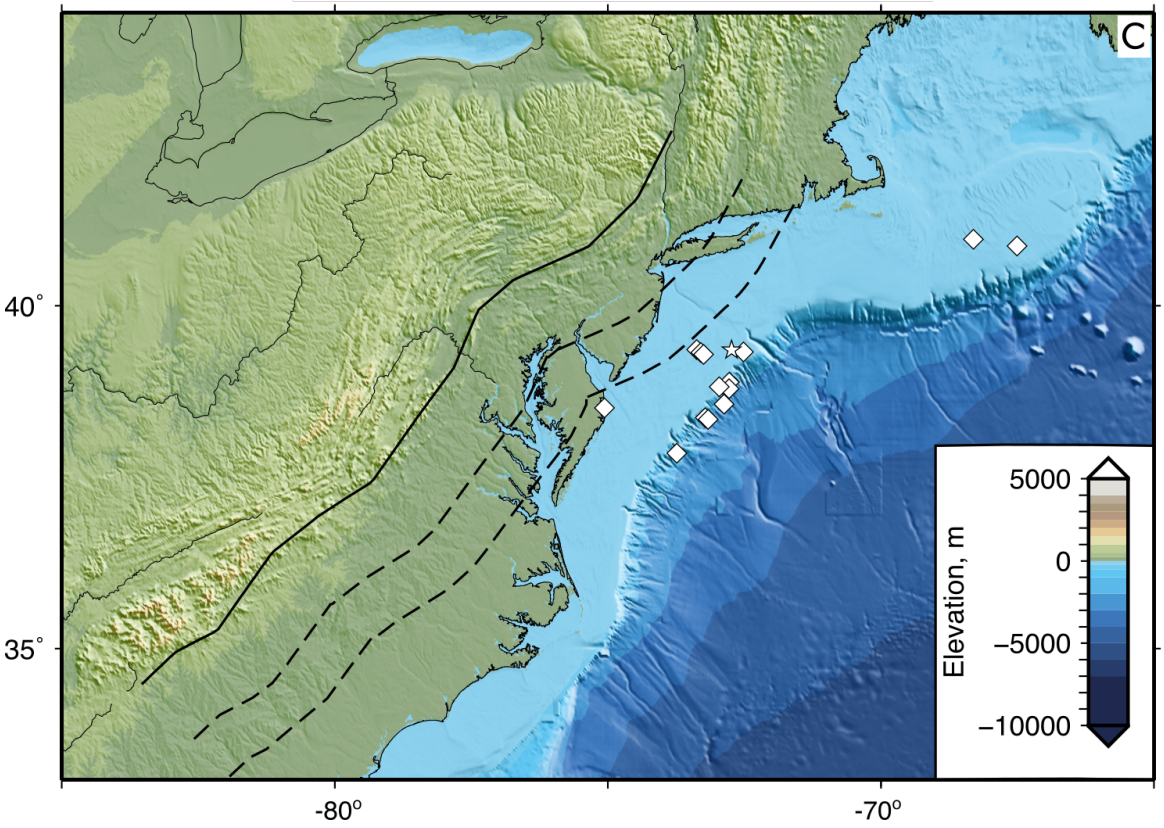

c
40°
35°
-80°
-70°
Elevation, m
5000
0
−5000
−10000

Figure 8: **Flexural analysis**. (a) Color scale = elastic thicknesses, T_e, from Audet (2014)'s spherical wavelet analysis of gravity and topography. $\circ$ = measurements on eastern seaboard used to generate histogram shown in panel (b). Blue circle encompasses Baltimore Canyon Trough (BCT). (b) Histogram of T_e estimates from eastern seaboard (white bars) and Baltimore Canyon Trough (blue). Note T_e of $\sim$ 15–40 km centered on Baltimore Canyon Trough. (c) Solid curve = eastern margin of the Appalachian mountains. Dashed curves show calculated distances to forebulge crests, which equal 128 and 216 km for elastic thicknesses T_e = 20 and 40 km, respectively. Note that all wells in this study (diamonds/star) sit outboard of the calculated forebulge positions.

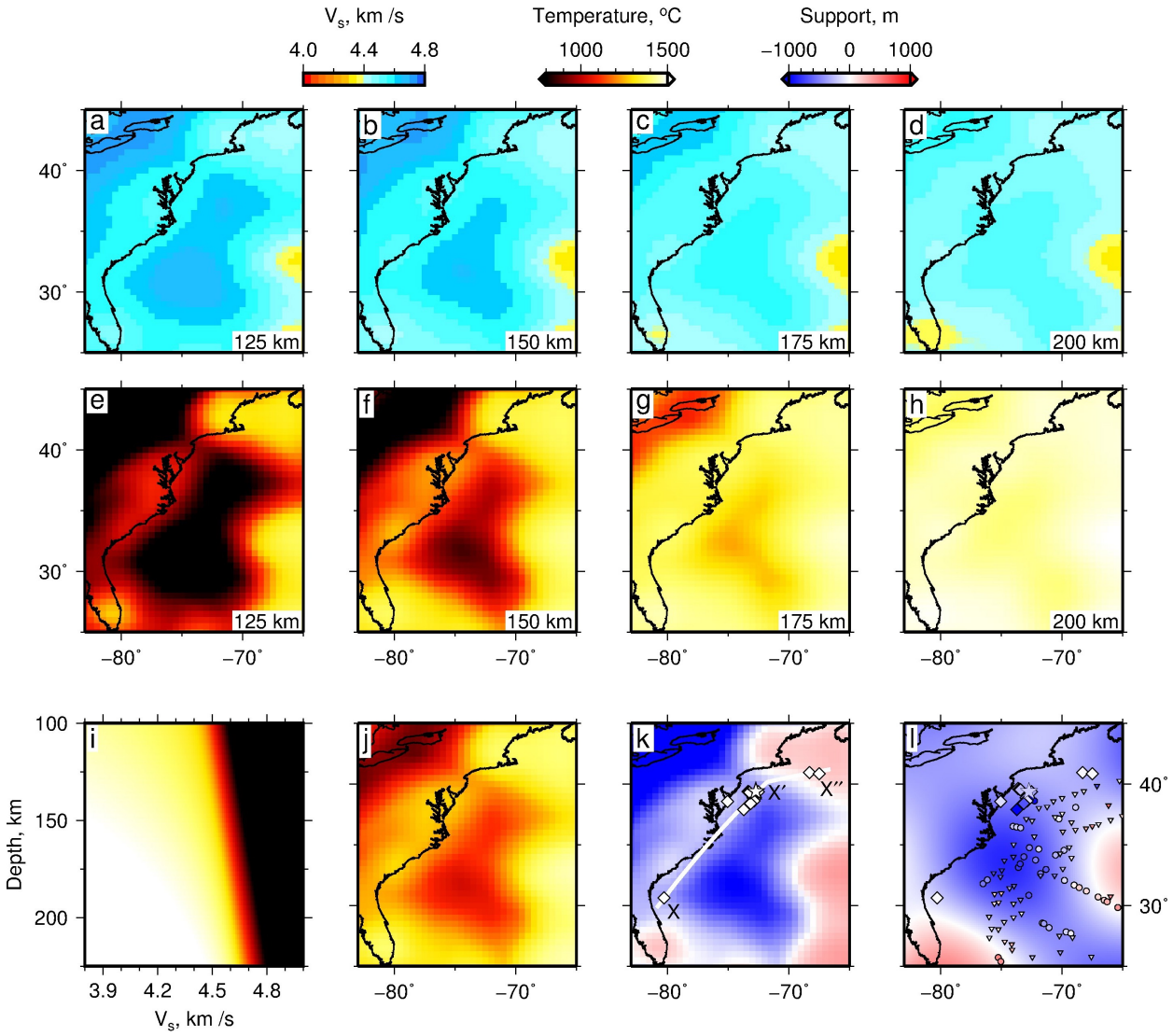


Figure 9: **Sub-plate drawdown of Eastern North America's passive margin.** (a–d) Slices through SL2013sv tomographic model, converted into absolute velocity using AK135 reference velocity model (Schaeffer and Lebedev, 2013). (e–h) Temperatures calculated using parameterization of Priestley and McKenzie (2006), see panel (i). (j) Average temperature between 125–200 km. (k) Calculated isostatic support from average excess (positive or negative) temperature anomalies between 125–200 km depth (see body text). White curve = transect shown in Figure 10; white diamonds/star = wells backstripped in this study (Figure 2). (l) Color scale = spherical harmonic model of dynamic topography up to degree $l = 30$ (Hoggard et al., 2017). Circles/downward pointing triangles = accurate/upper estimates of residual ocean-age depths (Hoggard et al., 2017). Colored diamonds and star show Neogene water-loaded subsidence from wells in this study (same color scale as calculated support; see Figures 2 & 5).

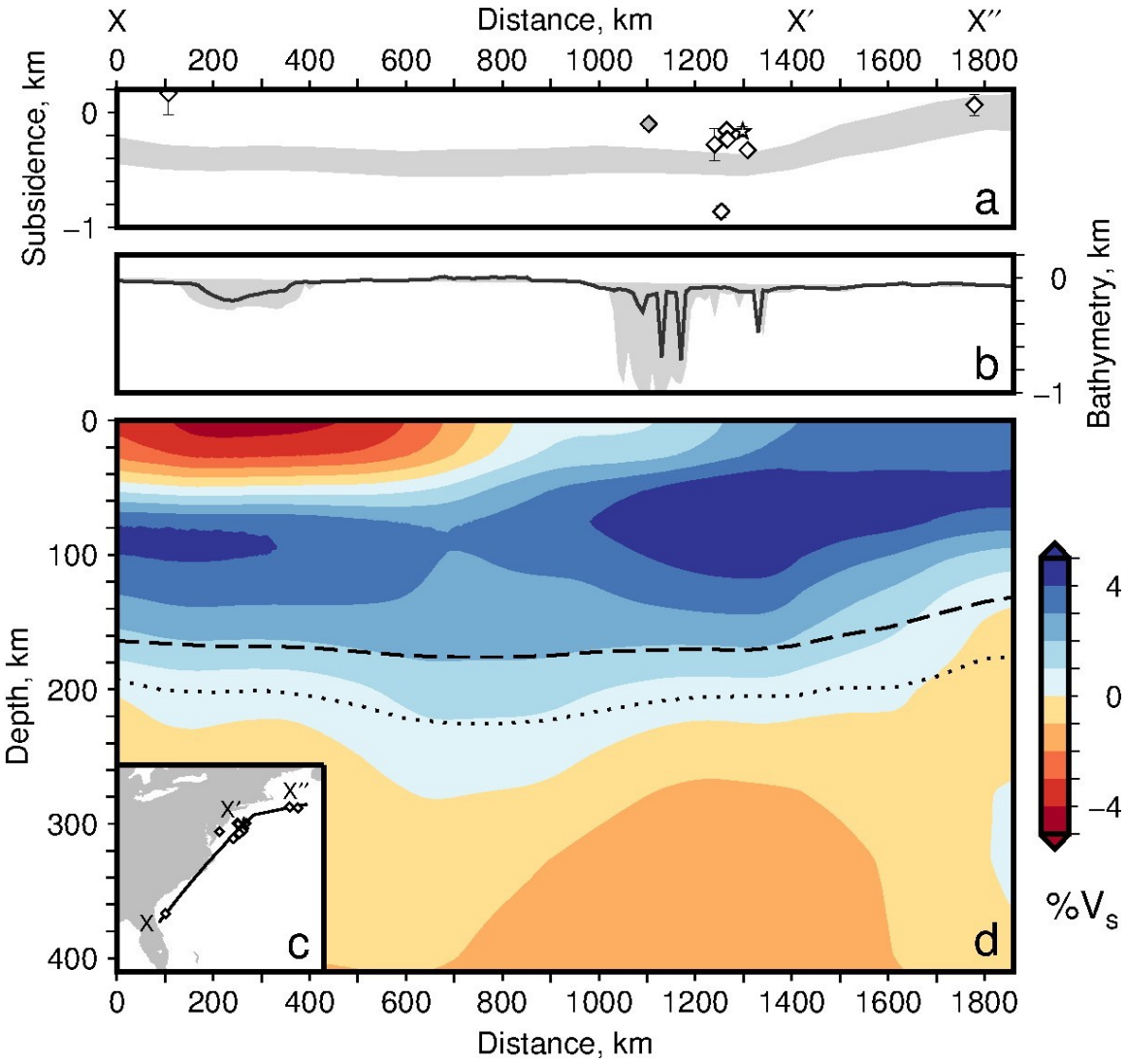


Figure 10: **Upper mantle drawdown of Eastern North America's passive margin.** (a) Gray band = upper mantle topographic support calculated along the transect shown in panel (c). Calculation was performed by converting the shear wave model of Schaeffer and Lebedev (2013) into temperature using the parameterization of Priestley & McKenzie (2006; PM06) and Goes et al. (2012; G12), and a simple isostatic calculation (see body text; Figure 9). Diamonds and star = Neogene water-loaded subsidence calculated by backstripping wells along the margin. Note that wells with scant Cenozoic stratigraphic records or no paleowater depth information were omitted from this plot. Star = COST B-2 well; gray diamond = onshore Bethany Beach well. Error bars = paleo-water depth uncertainties. (b) Topographic/bathymetric profile from ETOPO1 dataset. Gray band = extremal values within 200 km wide swath. (c) Location of transect (solid line) and wells backstripped in this study (diamonds/star; see Figures 2 & 9). (d) Vertical slice through the SL2013sv tomographic model of Schaeffer and Lebedev (2013) along the dog-leg transect. Dashed/dotted lines = position of calculated 1330°C isotherm (i.e. base of the plate) calculated using PM06/G12 parameterization.